NASA Technical Memorandum 104023

Accuracy of Tilt Rotor Hover Performance Predictions

Fort F. Felker

June 1993

National Aeronautics and
Space Administration

NASA Technical Memorandum 104023

Accuracy of Tilt Rotor Hover Performance Predictions

Fort F. Felker, Ames Research Center, Moffett Field, California

June 1993

National Aeronautics and
Space Administration

Ames Research Center
Moffett Field, California 94035-1000

Summary

The accuracy of various methods used to predict tilt rotor hover performance was established by comparing predictions with large-scale experimental data. A wide range of analytical approaches were examined. Blade lift was predicted with a lifting line analysis, two lifting surface analyses, and by a finite-difference solution of the full potential equation. Blade profile drag was predicted with two different types of airfoil tables and an integral boundary layer analysis. The inflow at the rotor was predicted using momentum theory, two types of prescribed wakes, and two free wake analyses. All of the analyses were accurate at moderate thrust coefficients. The accuracy of the analyses at high thrust coefficients was dependent upon their treatment of high sectional angles of attack on the inboard sections of the rotor blade. The analyses which allowed sectional lift coefficients on the inboard stations of the blade to exceed the maximum observed in two-dimensional wind tunnel tests provided better accuracy at high thrust coefficients than those which limited lift to the maximum two-dimensional value. These results provide tilt rotor aircraft designers guidance on which analytical approaches provide the best results, and the level of accuracy which can be expected from the best analyses.

Nomenclature

A	rotor disc area, πR^2, m^2
C_P	rotor power coefficient, $P/\rho A\Omega^3R^3$
C_T	rotor thrust coefficient, $T/\rho A\Omega^2R^2$
P	rotor power, N-m/s
R	rotor radius, m
r	radial distance from rotor axis, m
T	rotor thrust, N
z	axial distance from rotor hub, m
σ	rotor solidity
ρ	air density, kg/m^3
Ω	rotor rotation speed, rad/s

Introduction

Hover performance is one of the most important factors that determine the economic viability of tilt rotor aircraft. The rotor performance in hover usually determines the total installed power, or limits the payload. It is essential that accurate hover performance predictions be available to assess the total mission performance of any proposed tilt rotor aircraft. At the detail design stage, the performance analysis must be accurate enough to allow for selection of the optimum rotor design for a given application.

A wide range of analytical methods for predicting hover performance are available to the designer of a tilt rotor aircraft. The available choices range from simple momentum theory to solutions of the full Navier–Stokes equations. In general, the more sophisticated analyses are more difficult to use and require greater computational resources than the simpler analyses. In return, the more sophisticated analyses will hopefully provide more accurate results. However, it is usually unclear how much more accurate the sophisticated analyses are, and whether or not the increase in accuracy justifies the additional time and expense. Furthermore, it is also uncertain what level of accuracy is achieved by the best analyses.

This paper provides a critical assessment of the present capability to predict tilt rotor hover performance using a variety of analytical methods. The accuracy of each analytical method is established by comparing its predictions with large-scale test data. No special "tuning" of the analyses was done to improve the correlation with test data. Thus, the accuracy results presented here should be representative of what could be obtained for a new tilt rotor design, prior to the acquisition of test data.

As a ground rule, only analyses which were available in the public domain or were commercially available were considered. As a result, a number of excellent company-proprietary analyses were not examined. Most of the analyses which were used required the user to make many choices when setting up the input files. In all cases, the input files were set up following the recommendations in the codes' documentation, and no effort was made to modify the input files to achieve better correlation with the test data. The intent of this effort was to establish the accuracy which could be expected for true predictions: analysis conducted in the absence of test data for the configuration of interest. The author does not claim to be an expert user of any of the analyses, but the choices which were made were reasonable, and should be representative of the choices which would be made by a typical user in the absence of test data. The same airfoil tables were used for all analyses (if required), and these tables were defined based on two-dimensional wind tunnel test data, without any adjustment of drag coefficients.

The author is grateful to Dave Jordan of NASA Ames for providing access to LSAF, and to Dr. Krishna Ramachandran of Flow Analysis, Inc., for running the HELIX cases.

Analytical Methods

Five different analytical modeling approaches were considered for the prediction of isolated rotor performance in hover. They were a lifting-line method with a momentum theory uniform inflow (CAMRAD/JA (refs. 1 and 2)), a lifting-line method with a Kocurek–Tangler prescribed wake (also CAMRAD/JA), a lifting-surface method with a circulation-coupled prescribed wake (LSAF (ref. 3)), a lifting-surface method with a free wake (EHPIC (ref. 4)), and a computational fluid dynamics analysis which solves the full-potential equation with a Lagrangian potential wake model (HELIX (ref. 5)). CAMRAD/JA, LSAF, and EHPIC used airfoil tables to determine the airfoil sectional drag coefficient, and HELIX used an integral boundary layer analysis. The blades were assumed to be rigid in all analyses. This is a reasonable approximation, as CAMRAD/JA predicts less than 0.5 degrees of elastic twist at the tip for these rotors in hover.

Note that no analyses which solve the full Navier–Stokes equations were used for this effort. Although the Navier–Stokes analyses have been developed to the point where they provide considerable capability (ref. 6), their use requires large computational resources which make them impractical for design applications. It is anticipated that this limitation will eventually be overcome, and the Navier–Stokes analyses will then be used as design tools.

CAMRAD/JA

CAMRAD/JA used a second-order-accurate lifting-line to represent the rotor blade aerodynamics, with airfoil lift and drag coefficients found from table look-up based on the local sectional angle of attack and Mach number. Fifteen to twenty aerodynamic segments were used for the rotor blade lifting-line model. A variety of options were available within CAMRAD/JA for determining the rotor inflow. For this investigation the uniform inflow (determined from momentum theory) and nonuniform inflow (determined from the Kocurek–Tangler prescribed wake model (ref. 7), with the wake geometry a function of the thrust coefficient) options were used. Following typical practice with CAMRAD/JA, the uniform inflow was increased by 10% relative to the ideal momentum theory value. When the prescribed wake option was used, the far wake axial descent rate of the tip vortex (KWGT(2)) was reduced by 10% to compensate for the truncation of the tip vortex after 5 revolutions. The Kocurek–Tangler prescribed wake model is a function of the blade linear twist rate, and it is unclear what equivalent linear twist rate should be used for tilt rotor configurations, which have nonlinear twist distributions. Following reference 8, the equivalent linear twist rate was chosen to be the average twist rate over the outer 30% of the blade span. Because of this choice, the tip vortex geometry was computed externally to CAMRAD/JA (using the equations of ref. 7) and manually input to the analysis.

LSAF

LSAF used a lifting-surface method to model the rotor blade aerodynamics, with airfoil lift and drag coefficients found from table look-up based on the local section angle of attack and Mach number. Twenty spanwise and two chordwise panels were used to represent the rotor blade. The inflow was determined from a circulation-coupled prescribed wake method, with the geometry of the wake determined from the peak bound circulation on the rotor blade rather than the thrust coefficient. Wake expansion of the tip vortex was prescribed to occur at a 15° angle (the default value) after 4 blade passages. This was intended to model the gradual transition from a well-ordered vortex flow to a turbulent jet which occurs in actual rotor wakes.

EHPIC

EHPIC used a vortex-lattice method to model the rotor blade aerodynamics, which was equivalent to a constant-strength doublet lifting surface method. Four chordwise and 36 spanwise panels were used to represent the rotor blade. EHPIC defined the blade section lift coefficient using the section circulation from the vortex lattice method. Thus, the local angle of attack never entered into the problem, and the section profile drag coefficient must be found as a function of the lift coefficient and Mach number. To accomplish this, the standard C81-format airfoil tables, which define lift and drag coefficients as a function of angle of attack and Mach number, were transformed into a format which gives drag coefficient as a function of lift coefficient and Mach number only. Since the vortex-lattice method models potential flow, there was no fundamental limit to the lift coefficients which were predicted by the method, and lift coefficients in excess of the a section's two-dimensional maximum lift coefficient may be predicted. To model stall at these extreme lift coefficients EHPIC used a large drag coefficient, but did not limit the maximum lift coefficient. This feature of the analysis had a significant effect on the predicted hover performance.

The rotor inflow was calculated in EHPIC from a series of vortex filaments which represented the tip vortex and inboard sheet of the rotor wake. Seven or eight of these filaments were used for the present calculations. The

positions of these filaments were adjusted by the analysis to achieve a force-free wake configuration. The wake was effectively extended to infinity by using an analytical representation of the far wake. Thus, EHPIC used a true free wake, with none of the features of the wake geometry determined from experimental data.

HELIX

HELIX solves the full-potential equation on a finite-difference mesh which wraps around the rotor blade. Seventeen grid planes were used along the span of the blade, with a total of approximately 200,000 grid points. The wake geometry was modeled using a set of Lagrangian markers, with the vorticity associated with these markers smeared over several nearby grid points. The wake was computed as a part of the total solution, and is a true free wake. Blade profile drag was calculated using an integral boundary layer analysis. However, the boundary layer model was not able to handle separated flow. As will be seen in the section of this report containing HELIX results, the code's inability to handle cases with separated flow severely limits its utility for tilt rotors.

Experimental Data

The hover performance of three tilt rotor configurations was measured in a series of back-to-back tests at the Ames Outdoor Aerodynamic Test Facility. The rotors which were tested were the original metal blades for the XV-15 aircraft (XV-15 blades), a set of composite "Advanced Technology" blades for the XV-15 (ATB blades), and a 0.658-scale model of the blades used on the V-22 aircraft (V-22 blades). All three rotors had diameters of 25 feet, providing full-scale Reynolds numbers. The solidity of the rotors was 0.0891 for the XV-15, 0.103 for the ATB, and 0.1138 for the V-22. The rotors were tested at full-scale tip Mach numbers in very low winds. The results of these tests were summarized in Ref. 8, and the complete data sets, including definition of the planform, twist, and airfoils of each rotor, were provided in references 9–11. Data are available for a range of tip Mach numbers for each rotor, but for this investigation only data acquired at the normal operating tip Mach number for each rotor was used. These tip Mach numbers were 0.69 for the XV-15 rotor, 0.66 for the ATB rotor, and 0.68 for the V-22 rotor.

The experimental data (and analytical predictions) are presented in terms of power coefficient as a function of thrust coefficient, with both normalized by the rotor solidity ratio. An expanded scale is used, which concentrates on the range of thrust coefficients over which tilt rotor aircraft usually operate (henceforth, the terms "thrust coefficient" and "power coefficient" denote C_T/σ and C_P/σ, respectively). Alternatively, the results could be presented in terms of figure of merit as a function of thrust coefficient. However, this format has been avoided because it is difficult to present profile and induced components of power in a figure of merit format.

CAMRAD/JA Results with Uniform Inflow

Figure 1 shows a comparison of predicted and measured rotor performance in hover using CAMRAD/JA with uniform inflow. Figure 1(a) shows results for the XV-15 rotor, figure 1(b) shows results for the ATB rotor, and figure 1(c) shows results for the V-22 rotor. The results for all three rotors were good for thrust coefficients of 0.14 or less. However, as the thrust coefficient was increased past this value, the power of the XV-15 and ATB rotors was overpredicted by a wide margin. The errors were especially large for the XV-15 rotor, where the power was overpredicted by 14 percent at a thrust coefficient of 0.165.

The same phenomenon was responsible for the sharp increase in predicted power as the thrust coefficient was increased for both the XV-15 and ATB rotors. The analysis indicated that the inboard sections of the rotor blade were operating at sectional angles of attack well above their two-dimensional stall angle. The stall angle is taken to be the minimum angle of attack for which the lift curve slope is zero. The sectional profile drag coefficients of these stalled airfoil sections were very large. Figure 2 shows the sectional angle of attack distribution predicted by CAMRAD/JA with uniform inflow, and figure 3 shows the associated profile drag coefficients, for the XV-15 rotor at a thrust coefficient of 0.153. The very large profile drag coefficients on the inboard sections of the rotor were responsible for the sharp increase in power as the thrust coefficient was increased. The effect of these large drag coefficients on the rotor power is shown in figure 4, which is a plot of the XV-15 rotor profile, induced, and total power coefficients as a function of thrust coefficient. The sharp increase in profile power was responsible for the sharp increase in total power at the higher thrust coefficients. This phenomenon was not observed in the comparisons of predicted and measured performance for the V-22 rotor (fig. 1(c)), because the V-22 airfoils have higher maximum lift coefficients than the XV-15 or ATB airfoils, and because the test data do not extend to extremely high thrust coefficients for the V-22 rotor.

One of the most important choices to be made when using CAMRAD/JA with the uniform inflow option is how much to increase the inflow over the minimum value

defined by momentum theory. For the calculations presented here, the inflow was increased by 10 percent over the momentum theory value. To show the influence of this choice on the predicted performance, figure 5 presents a comparison of the predictions obtained with the V-22 rotor when increasing the inflow by 10 percent and 15 percent. The good correlation obtained between the predictions and test data at low thrust coefficients for all three rotors (figs. 1(a–c)) indicates that the baseline 10 percent increase is a reasonable choice for tilt rotors. A small improvement in accuracy could be obtained by using larger values at the highest thrust coefficients.

CAMRAD/JA Results with Prescribed Wake

Figure 6 shows a comparison of predicted and measured rotor performance in hover using CAMRAD/JA with the nonuniform inflow prescribed wake. Figure 6(a) shows results for the XV-15 rotor, figure 6(b) shows results for the ATB rotor, and figure 6(c) shows results for the V-22 rotor. The results were generally similar to those obtained using uniform inflow, with good results obtained for the V-22 rotor, but with the power substantially overpredicted for the XV-15 and ATB rotors at high thrust coefficients. However, the sharp increase in power at the higher thrust coefficients was more severe in this case than for the uniform inflow case (compare figs. 1(a) and 6(a), or figs. 1(b) and 6(b)).

Figure 7 shows that the poorer results obtained with the prescribed wake analysis were caused by increases in both the profile and induced power relative to the uniform inflow predictions. The increases in the induced power were caused by the highly nonuniform (and therefore nonoptimal) induced velocity at the rotor disc associated with the vortex wake. This nonuniform inflow is also responsible for the increased profile power. This is because the nonuniform inflow from the prescribed wake, when compared with uniform inflow, tends to predict relatively lower inflow on the inboard sections of the rotor, and relatively higher inflow on the outboard sections of the rotor. The lower inflow on the inboard sections results in higher angles of attack (fig. 8), which lead to higher drag coefficients (fig. 9). These extremely large drag coefficients were again responsible for the sharp increase in predicted profile power at high thrust coefficients.

The tip vortex geometry data provided in reference 8 for the ATB rotor provide an opportunity to check the wake geometry used in the prescribed wake model. Figure 10 shows a comparison of predicted and measured tip vortex geometry, with figure 10(a) showing the axial and figure 10(b) showing the radial geometry.

The initial tip vortex axial descent rate (for wake azimuth angles between 0 and 60 degrees) was overpredicted. However, the axial position of the tip vortex at the first blade passage, which has a significant influence on the blade radial loading distribution, was well predicted. The far wake (wake azimuth angles greater than 120 degrees) axial descent rate was slightly underpredicted, but recall that the rate used by CAMRAD/JA was deliberately reduced by 10 percent to compensate for the truncation of the tip vortex after five revolutions. Overall, the comparison of the predicted and measured tip vortex axial geometry was very good, and the observed errors in the predicted rotor performance were not caused by the slight differences between the theory and the wake geometry shown in figure 10(a).

The comparison between the predicted and measured tip vortex radial geometry was less satisfactory. The radial contraction of the tip vortex was underpredicted for the entire range of wake azimuth angles. The predicted radial location of the tip vortex at first blade passage was about 2 percent of the rotor radius further outboard than measured. This error affects the details of the blade radial loading distribution near the tip of the blade. To assess the effect of the underprediction of the tip vortex contraction on the predicted rotor performance, CAMRAD/JA was rerun with the prescribed wake adjusted to match the observed tip vortex contraction. The resulting predictions of rotor power were 2–3 percent lower than those obtained with the standard Kocurek–Tangler wake geometry, which was a small change relative to the 20 percent error in the predicted power at this thrust coefficient (fig. 6(b)). Thus, it has been shown that the small differences between the predicted and measured wake geometry cannot account for the large errors in the predicted power at high thrust coefficients for the ATB rotor. This result is consistent with the findings reported in reference 8.

LSAF Results

Figure 11 shows a comparison of predicted and measured rotor performance in hover using LSAF. Figure 11(a) shows results for the XV-15 rotor, figure 11(b) shows results for the ATB rotor, and figure 11(c) shows results for the V-22 rotor. These results differ very little from those obtained with CAMRAD/JA when the prescribed wake option was used (see figs. 12(a–c)).

There are a number of similarities between the CAMRAD/JA prescribed wake model and that of LSAF. They are both based on the Kocurek–Tangler wake model, although LSAF bases the wake geometry on the maximum bound circulation instead of the thrust coefficient which is used in CAMRAD/JA. However,

they differ considerably in their treatment of the far wake. CAMRAD/JA truncates the tip vortex after 5 revolutions, with the far wake axial descent rate reduced by 10 percent to compensate. LSAF uses a more realistic far wake expansion model to represent the transition of the orderly helical vortex wake into a turbulent jet. For the blade aerodynamics, CAMRAD/JA uses a second-order-accurate lifting line theory while LSAF uses a lifting surface analysis. Both codes used identical airfoil tables for profile drag. Clearly, the similarities between the two analyses are far more significant than their differences, since their results are virtually indistinguishable for these three tilt rotors.

EHPIC Results

Figure 13 shows a comparison of predicted and measured rotor performance in hover using EHPIC, a free-wake analysis. Figure 13(a) shows results for the XV-15 rotor, figure 13(b) shows results for the ATB rotor, and figure 13(c) shows results for the V-22 rotor. Good results were obtained for all three rotors, with errors in the predicted power ranging from zero to six percent.

Figure 14 shows a comparison of the induced and profile power predicted for the XV-15 rotor using EHPIC and CAMRAD/JA with the prescribed wake. The induced power predicted by EHPIC is somewhat lower than that predicted by the prescribed wake model. The induced power predicted by the prescribed wake analysis is almost certainly too large, since the predicted induced power alone equals the measured total power at high thrust coefficients.

The EHPIC predictions of profile power show no sign of the sharp power increase associated with inboard blade stall which were exhibited by the CAMRAD/JA predictions. However, this is not because EHPIC predicts that the sectional angle of attack on the inboard sections is below the stall angle. Figure 15 shows a comparison of the predicted lift coefficients on the XV-15 blade at a thrust coefficient of 0.153, using EHPIC and CAMRAD/JA with the prescribed wake. The prescribed wake analysis predicts lift coefficients slightly above the nominal value of the stall lift coefficient on the inboard sections of the rotor because of nonlinear behavior of the blade root airfoil at angles of attack above stall (recall that stall was defined to occur at the lowest angle of attack for which the lift curve slope equals zero). EHPIC predicts lift coefficients well in excess of the stall lift coefficient. This is because EHPIC computes the lift coefficient from the bound circulation on the vortex lattice, and not from table look-up based on angle of attack. There is no fundamental limit to the lift coefficients which can be predicted by EHPIC, so that lift coefficients well in excess of an airfoil's two-dimensional maximum lift coefficient can be obtained.

EHPIC's only representation of stall is in the drag coefficients used by the analysis for lift coefficients in excess of the two-dimensional maximum lift coefficient of the airfoil. These drag coefficients are defined from an equivalent angle of attack which is found from the predicted lift coefficient and an unstalled lift curve slope. For example, if the predicted lift coefficient was 50 percent greater than the airfoil's two-dimensional maximum lift coefficient, then the associated drag coefficient would be found from the C81 table at an angle of attack 50 percent greater than the angle of the maximum lift coefficient. A comparison of the predicted drag coefficients on the XV-15 blade at a thrust coefficient of 0.153, using EHPIC and CAMRAD/JA with the prescribed wake, is shown in figure 16. The lower drag coefficients predicted using EHPIC are responsible for the lower profile power shown in figure 14.

The prediction by EHPIC of lift coefficients greater than a 2-D section's maximum lift coefficient is troubling, and the code was set up to allow this merely because it was a convenient choice for the code's developers. The developers recognized this as a limitation of the analysis, and work is underway to eliminate this problem in the next release of the software. However, a number of factors indicate that the inboard sections of a tilt rotor blade do, in fact, maintain attached flow at angles of attack well above the 2-D section's stall angle of attack, producing very high lift coefficients.

Tung and Branum (ref. 12) provide experimental evidence of attached flow, and consequently very high lift coefficients, on the inboard sections of a model tilt rotor blade at high thrust coefficients. Lift coefficients of over 2.7 were measured at a radial station of 0.125 R, and lift coefficients of over 1.7 were measured at a radial station of 0.2 R. These lift coefficients were well in excess of the airfoil sections' 2-D maximum lift coefficient, which cannot be much greater than 1 for the low Reynolds numbers of the small-scale rotor which was tested. There was no evidence of flow separation at these inboard stations. Himmelskamp (ref. 13) obtained similar results for a model propeller. Narramore and Vermeland (ref. 14) conducted a computational study of the V-22 rotor blade using the 3-D Navier–Stokes equations. They obtained results which were consistent with the experimental data of Tung and Branum, with very high lift coefficients and no flow separation on the inboard sections of the rotor. However, their results were severely compromised by the inadequate grid resolution in the boundary layer. The reason for the observed behavior is unclear, although reference 14 shows that radial flow in the boundary layer

is not a factor. This is an area that is ripe for additional research.

Thus, there is a substantial body of evidence, both experimental and computational, which suggests that the inboard sections of a tilt rotor blade do not stall in a manner consistent with two-dimensional flow. EHPIC's blade aerodynamics model, although suspect at initial examination, may in fact be appropriate for tilt rotor blades. The good correlation between the predicted and measured rotor performance obtained with EHPIC is directly attributable to EHPIC's refusal to allow blade sections to stall. These results lend additional support to the idea that tilt rotor blades are able to maintain attached flow over their inboard sections at very large angles of attack.

A comparison of the predicted and measured wake geometry for the ATB rotor at a thrust coefficient of 0.17 is shown in figure 17. Figure 17(a) shows the axial wake geometry, and figure 17(b) shows the radial wake geometry. The initial axial descent rate (for wake azimuth angles between 0 and 60 degrees) was overpredicted, but the axial position at first blade passage was well-predicted by the free-wake analysis. The subsequent far-wake axial descent rate (wake azimuth angles greater than 120 degrees) was slightly under-predicted. This small error would not have a large effect on the performance predictions. The agreement between the predicted and measured tip vortex radial position was very good. These results provide confidence that the free-wake model correctly predicted the rotor wake configuration, and that the resulting predictions of inflow and induced power were correct.

HELIX Results

Figure 18 shows a comparison of predicted and measured rotor performance in hover using HELIX. Figure 18(a) shows results for the XV-15 rotor and figure 18(b) shows results for the ATB rotor (the V-22 rotor was not considered because of the difficulty of defining a grid for this rotor).

The predictions for the XV-15 rotor are in excellent agreement with the test data for the limited range of thrust coefficients covered by the analysis. The HELIX predictions of total power do not extend past thrust coefficients higher than 0.125, although the induced power was predicted for thrust coefficients as high as 0.170. This is because the integral boundary layer analysis in HELIX predicts the onset of separation at thrust coefficients above 0.125. The boundary layer model is unable to provide predictions of profile power in the presence of separation, and the total power coefficient of the XV-15 rotor cannot be predicted by HELIX for thrust coefficients above 0.125. It might be possible to estimate the profile power at higher thrust coefficients by, for example, assuming that the profile power was proportional to the square of the thrust coefficient. However, such a procedure would be inconsistent with the level of accuracy and sophistication provided by the finite-difference solution of the full-potential equation used for the inviscid portion of the analysis.

The results obtained for the ATB rotor are shown in figure 18(b). The power was slightly underpredicted over the range of thrust coefficients for which results were obtained. As for the XV-15 rotor, HELIX was not able to predict total power after the onset of separation, and results were not obtained for thrust coefficients greater than 0.16.

Figure 19 compares the profile power predictions of HELIX with EHPIC and LSAF. Figure 19(a) shows results for the XV-15 rotor and figure 19(b) shows results for the ATB rotor. The HELIX predictions are shown with the solid line, LSAF with the dotted line, and EHPIC results are shown by the dashed line. For the limited range of thrust coefficients for which HELIX was able to predict profile power, the results are in fair agreement with those of the other analyses. However, it is disturbing that the HELIX prediction shows the profile power to be decreasing with increasing thrust coefficient, instead of the expected increase in profile power with increasing thrust coefficient.

Figure 20 shows that the induced power predicted by HELIX for the XV-15 rotor is in good agreement with the predictions of various other analyses over the entire range of thrust coefficients. The HELIX predictions are shown with the solid line, CAMRAD/JA with uniform inflow by the dot-dash line, LSAF with the dotted line, and EHPIC results are shown by the dashed line. These results provide confidence in the induced power results obtained with HELIX for a tilt rotor configuration. Also, the good agreement on induced power among the various analyses, coupled with the lack of agreement on profile power, again confirms that the correct prediction of profile power is the key to obtaining accurate predictions of tilt rotor hover performance.

Conclusions

The accuracy of various methods used to predict tilt rotor hover performance was established by comparing predictions with large-scale experimental data. A wide range of analytical approaches were examined, and no special "tuning" of the analyses was performed to improve the correlation with test data. The accuracy of the results

should therefore be representative of what would be obtained in the absence of test data. Specific conclusions from this investigation were:

1. The predictions of hover performance were generally conservative, with the predicted power greater than the measured power, particularly at high thrust coefficients.

2. The total power results obtained with LSAF and CAMRAD/JA with the prescribed wake option were virtually identical.

3. The results acquired with HELIX were severely limited by the boundary-layer model's inability to handle separated flow. In its present form, this code is not useful for tilt rotor performance design studies.

4. All of the analyses provided good results for thrust coefficients which were low enough to keep all sections of the rotor blade at angles of attack below their 2-D stall angles of attack. As the thrust coefficient was increased past that point, the accuracy of each analysis was dependent upon its treatment of airfoil section lift and drag at very high angles of attack.

5. EHPIC, which allowed sectional lift coefficients on the inboard stations of the blade to exceed the maximum observed in two-dimensional wind tunnel tests, provided better accuracy at high thrust coefficients than the analyses which limit lift to the maximum two-dimensional value.

6. This result provides additional evidence to support the hypothesis that the inboard stations on tilt rotor blades maintain attached flow at very high angles of attack. The resulting high section lift coefficients and low drag coefficients allow these rotors to provide excellent performance at very high thrust coefficient to solidity ratios. Additional analytical and experimental work is required to provide a fundamental understanding of this phenomena, and to guide the development of a more accurate hover performance analysis for tilt rotors.

7. These results shown that EHPIC would probably provide the most accurate hover performance predictions for new tilt rotor designs. The predicted performance should be regarded as a conservative estimate, with the power overpredicted by zero to six percent at typical hovering thrust coefficients.

References

1. Johnson, W.: Development of a Comprehensive Analysis for Rotorcraft. Vertica, vol. 5, nos. 2 and 3, 1981.

2. Johnson, W.: A Comprehensive Analytical Model of Rotorcraft Aerodynamics and Dynamics. NASA TMs 81182–81184, June 1980.

3. Kocurek, J. D.; Berkowitz, L. F.; and Harris, F. D.: Hover Performance Methodology at Bell Helicopter Textron. Proceedings of the 36th Annual Forum of the American Helicopter Society, Washington, D.C., May 1980.

4. Quackenbush, T. R.; Bliss, D. B.; Wachspress, D. A.; and Ong, C. C.: Free Wake Analysis of Hover Performance Using a New Influence Coefficient Method. NASA CR-4309, July 1990.

5. Ramachandran, K.; Tung, C.; and Caradonna, F. X.: Rotor Hover Performance Prediction Using a Free-Wake, Computational Fluid Dynamics Method. Journal of Aircraft, vol. 26, no. 12, December 1989.

6. Srinivasan, G. R.; Raghavan, V.; and Duque, E. P. N.: Flowfield Analysis of Modern Helicopter Rotors in Hover by Navier–Stokes Method. Proceedings of the International Technical Specialists' Meeting on Rotorcraft Acoustics and Rotor Fluid Dynamics, Philadelphia, Pennsylvania, October 1991.

7. Kocurek, J. D.; and Tangler, J. L.: A Prescribed Wake Lifting Surface Hover Performance Analysis. Proceedings of the 32nd Annual Forum of the American Helicopter Society, Washington, D.C., May 1976.

8. Felker, F. F.; Maisel, M. D.; and Betzina, M. D.: Full-Scale Tilt-Rotor Hover Performance. Journal of the American Helicopter Society, vol. 31, no. 2, April 1986.

9. Felker, F. F.; Betzina, M. D.; and Signor, D. B.: Performance and Loads Data from a Hover Test of a Full-Scale XV-15 Rotor. NASA TM-86833, November 1985.

10. Felker, F. F.; Young, L. A.; and Signor, D. B.: Performance and Loads Data from a Hover Test of a Full-Scale Advanced Technology XV-15 Rotor. NASA TM-86854, January 1986.

11. Felker, F. F.; Signor, D. B.; Young, L. A.; and Betzina, M. D.: Performance and Loads Data from a Hover Test of 0.658-Scale V-22 Rotor and Wing. NASA TM-89419, April 1987.

12. Tung, C.; and Branum, L.: Model Tilt Rotor Hover Performance and Surface Pressure Measurement. Proceedings of the 46th Annual Forum of the American Helicopter Society, Washington, D.C., May 1990.

13. Himmelskamp, H.: Profile Investigations of a Rotating Airscrew. Reports and Translations No. 832, September 1947.

14. Narramore, J. C.; and Vermeland, R.: Use of Navier–Stokes Code to Predict Flow Phenomena Near Stall as Measured on a 0.658-Scale V-22 Tiltrotor Blade. AIAA Paper 89-1814, June 1989.

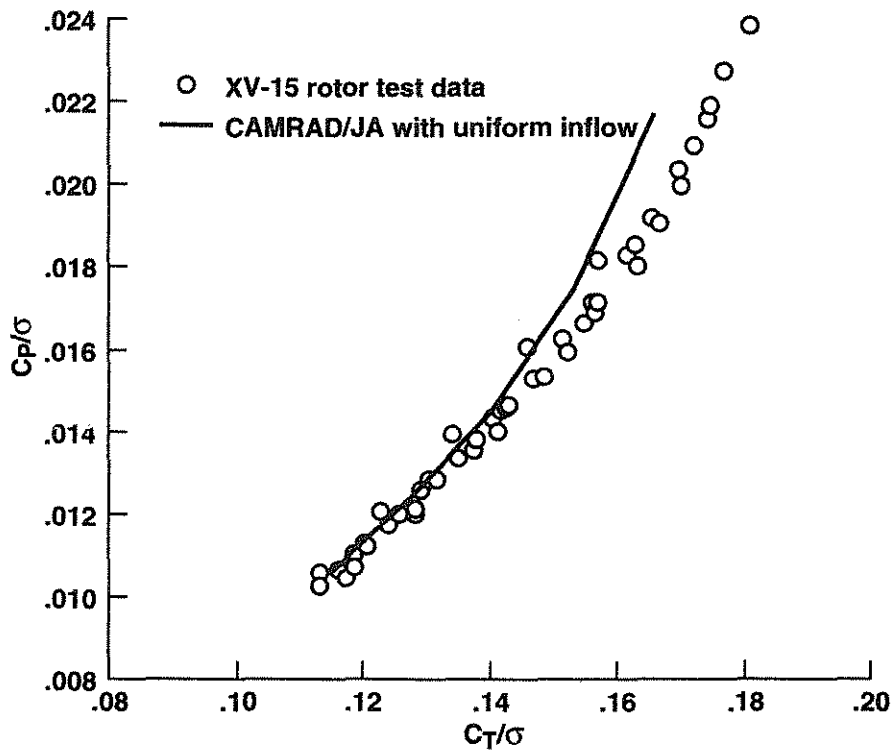

Figure 1(a). Comparison of CAMRAD/JA uniform inflow hover performance predictions with XV-15 rotor test data.

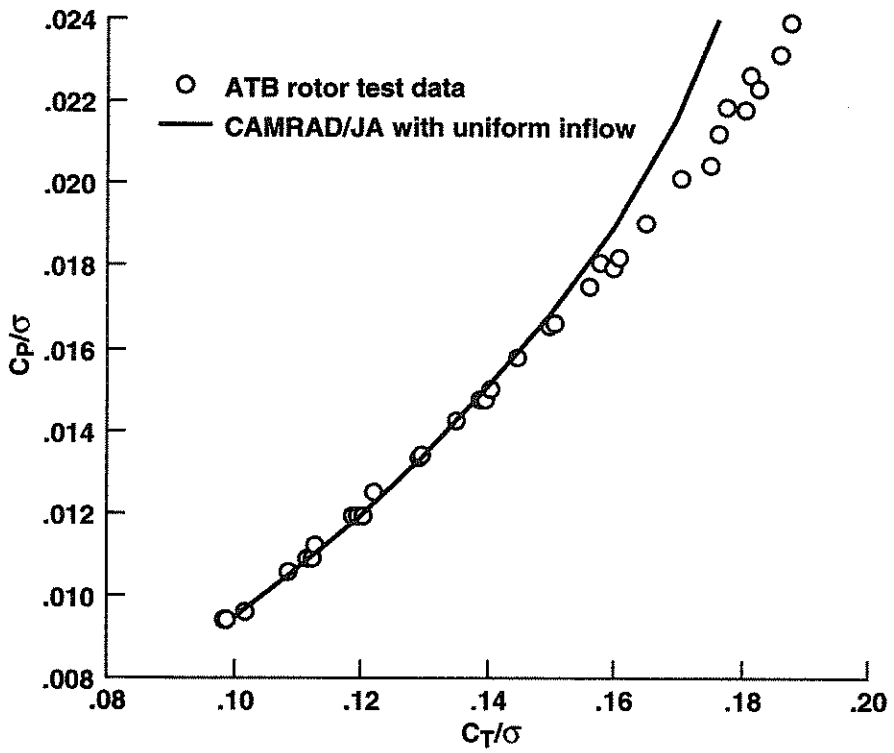

Figure 1(b). Comparison of CAMRAD/JA uniform inflow hover performance predictions with ATB rotor test data.

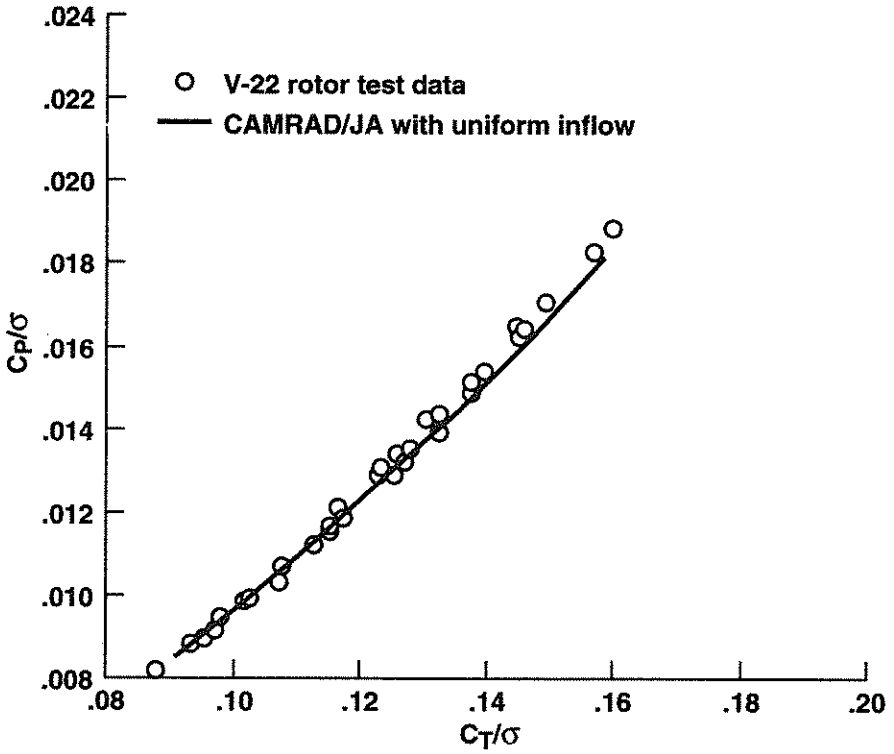

Figure 1(c). Comparison of CAMRAD/JA uniform inflow hover performance predictions with V-22 rotor test data.

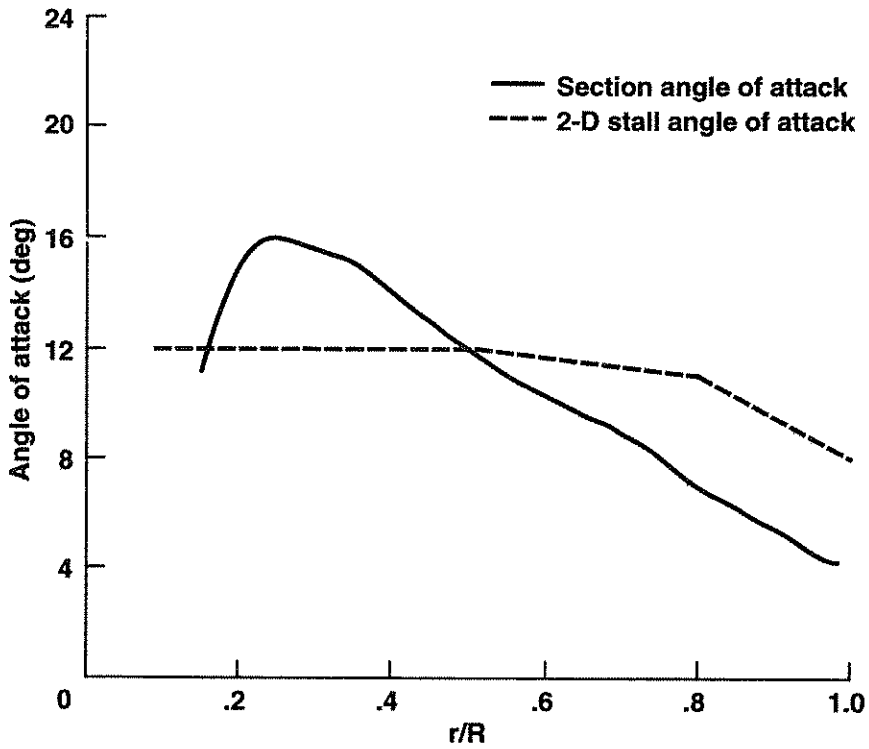

Figure 2. Predicted sectional angle of attack distribution, XV-15 rotor, $C_T/\sigma = 0.153$. Prediction from CAMRAD/JA with uniform inflow.

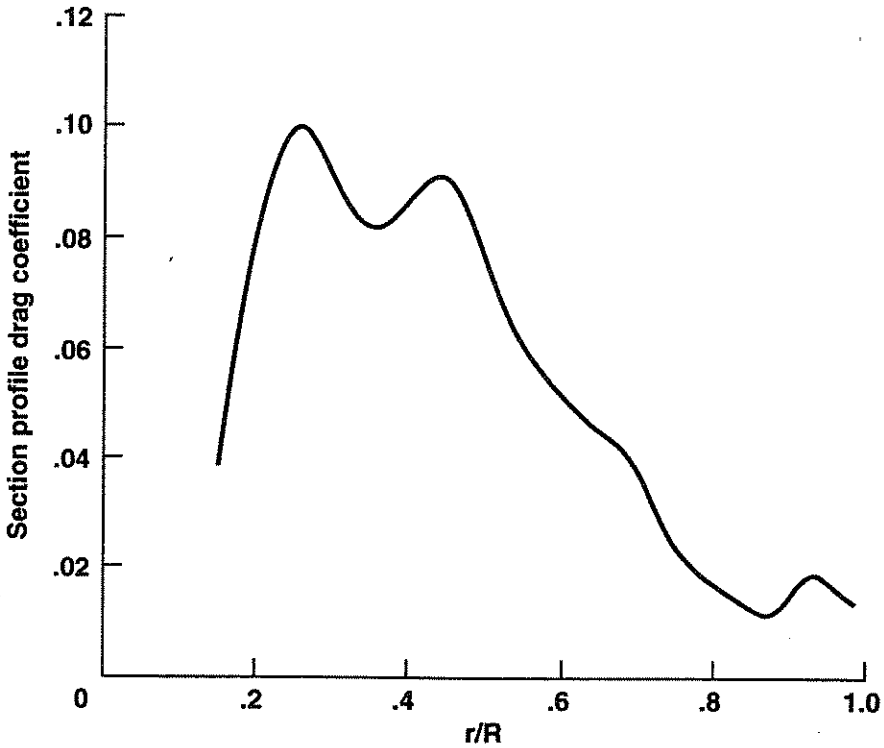

Figure 3. Predicted sectional drag coefficient, XV-15 rotor, $C_T/\sigma = 0.153$. Prediction from CAMRAD/JA with uniform inflow.

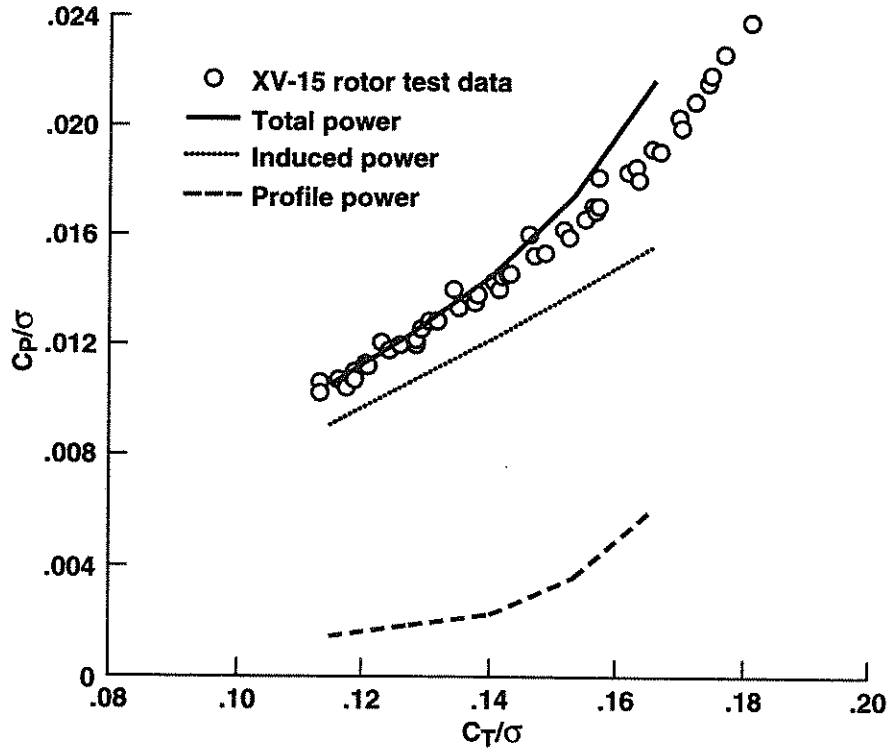

Figure 4. Predicted total, induced, and profile power coefficients, XV-15 rotor, $C_T/\sigma = 0.153$. Prediction from CAMRAD/JA with uniform inflow.

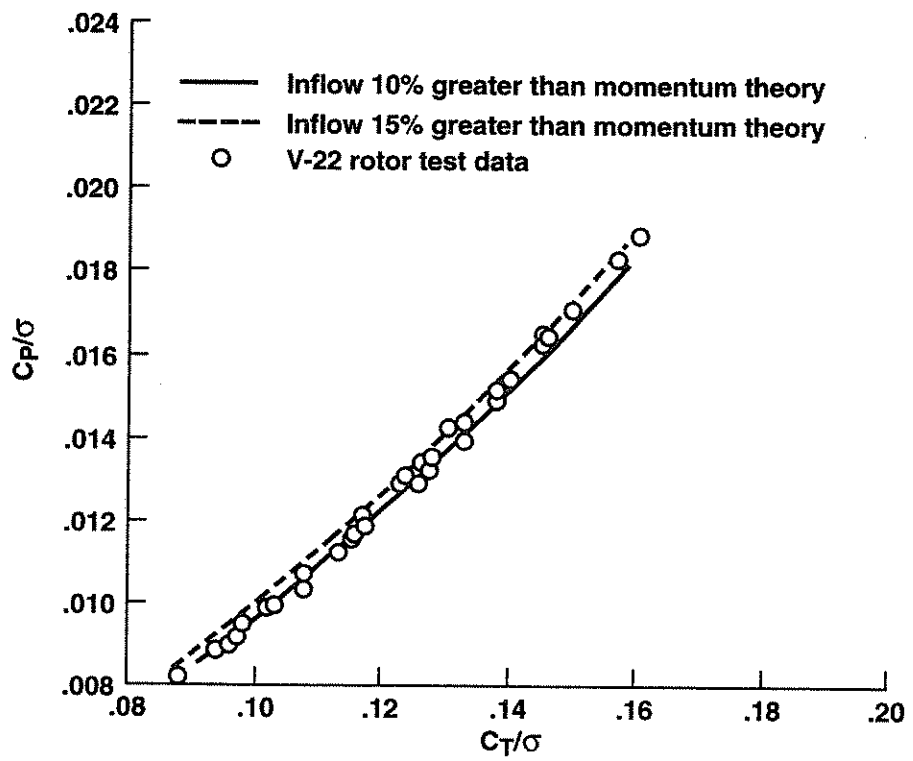

Figure 5. Effect of increased inflow on predicted rotor performance in hover. CAMRAD/JA with uniform inflow.

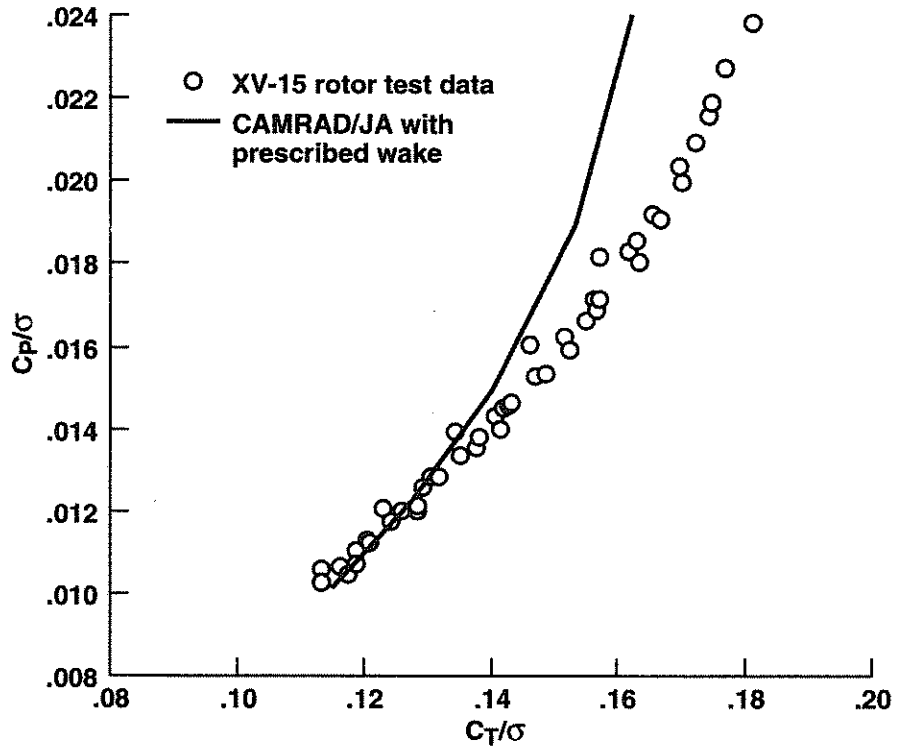

Figure 6(a). Comparison of CAMRAD/JA prescribed wake hover performance predictions with XV-15 rotor test data.

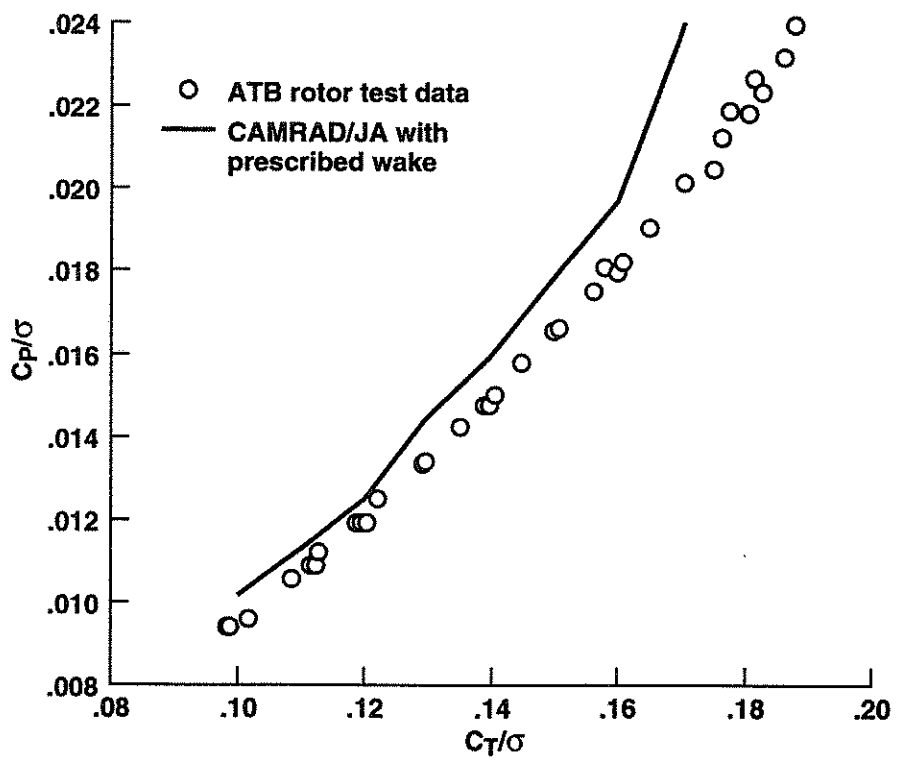

Figure 6(b). Comparison of CAMRAD/JA prescribed wake hover performance predictions with ATB rotor test data.

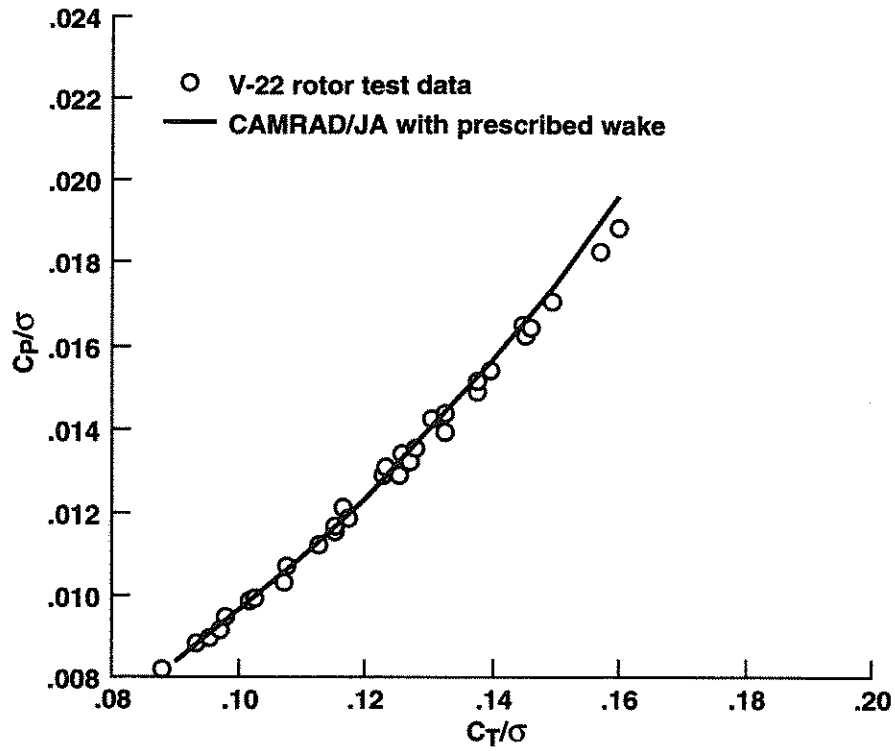

Figure 6(c). Comparison of CAMRAD/JA prescribed wake hover performance predictions with V-22 rotor test data.

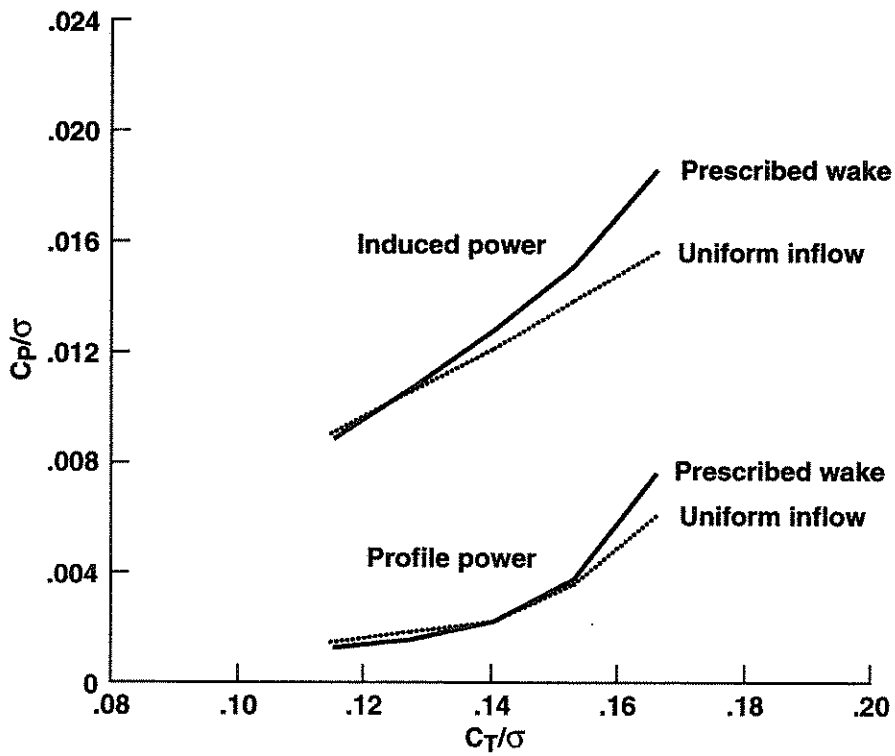

Figure 7. Comparison of induced and profile power predicted using CAMRAD/JA with uniform inflow and prescribed wake models. XV-15 rotor.

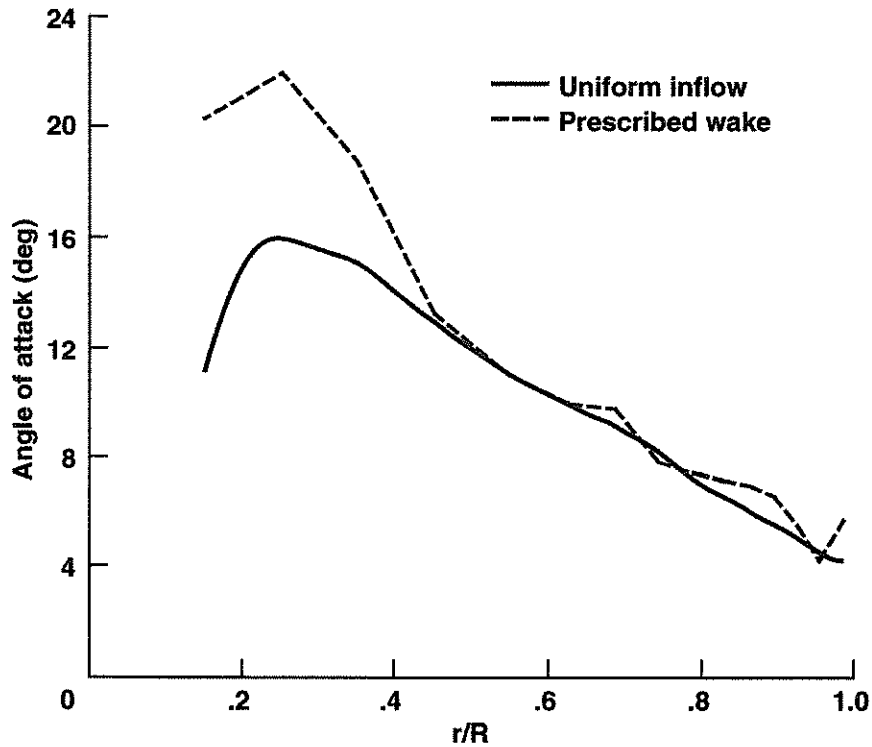

Figure 8. Comparison of sectional angle of attack distribution predicted using CAMRAD/JA with uniform inflow and prescribed wake. XV-15 rotor, $C_T/\sigma = 0.153$.

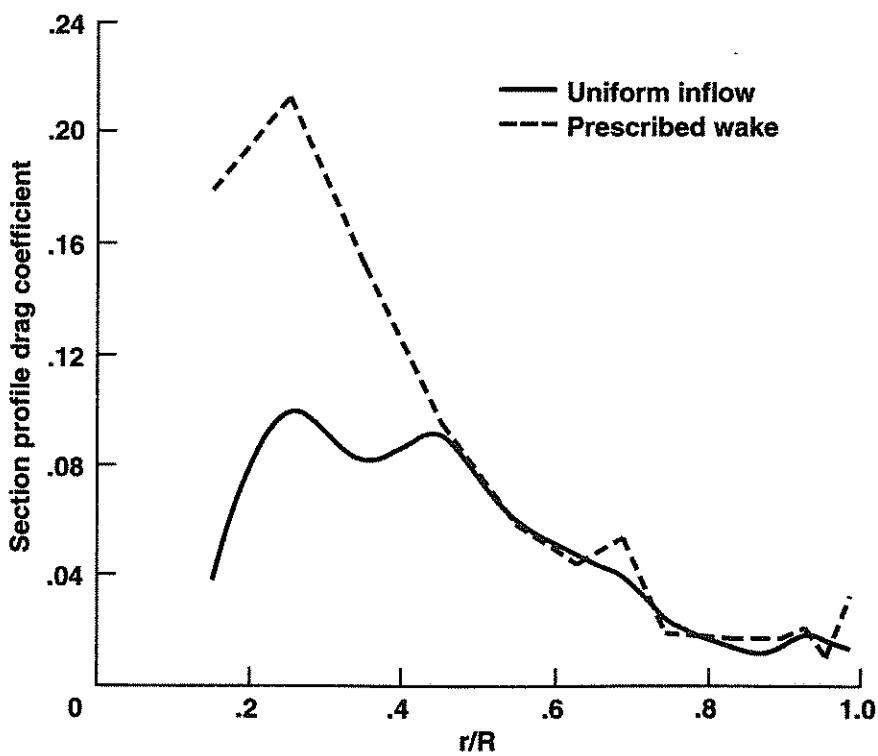

Figure 9. Comparison of sectional drag coefficient distribution predicted using CAMRAD/JA with uniform inflow and prescribed wake. XV-15 rotor, $C_T/\sigma = 0.153$.

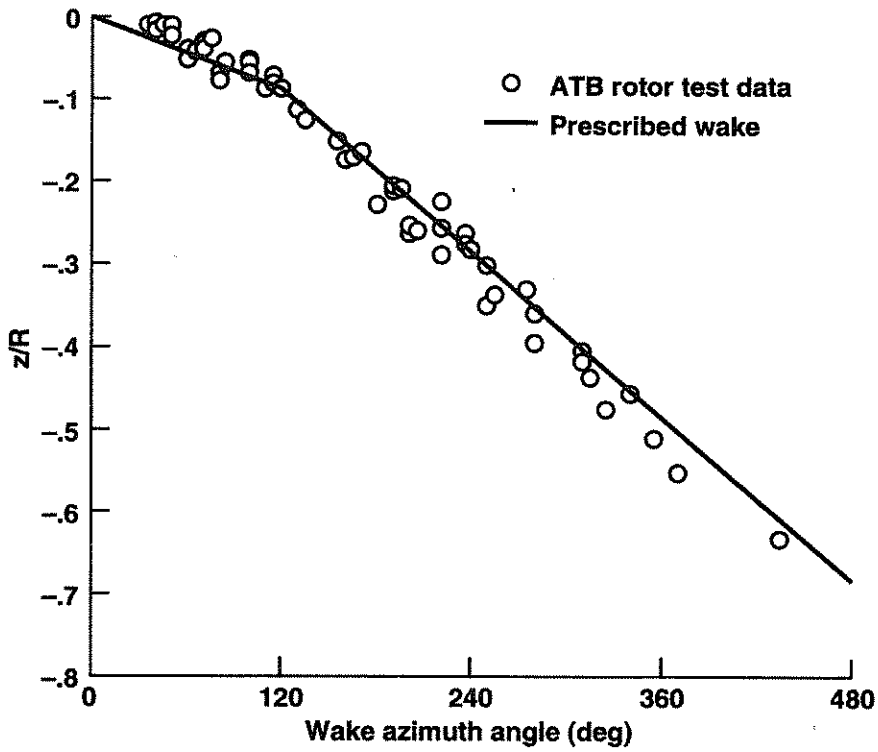

Figure 10(a). Comparison of prescribed wake tip vortex axial geometry with test data. ATB rotor, $C_T/\sigma = 0.17$.

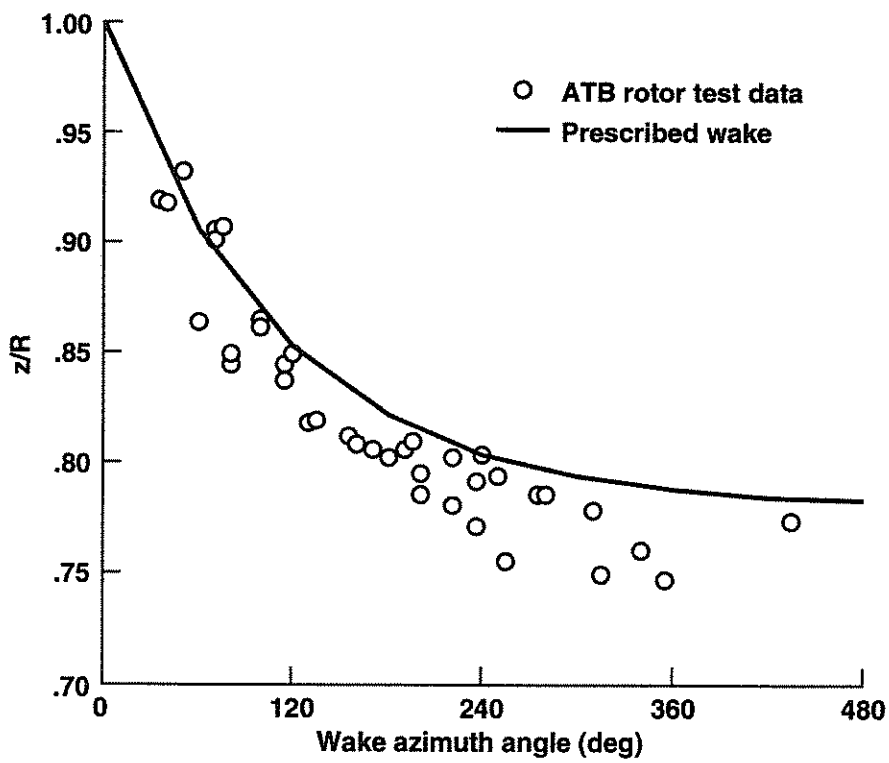

Figure 10(b). Comparison of prescribed wake tip vortex radial geometry with test data. ATB rotor, $C_T/\sigma = 0.17$.

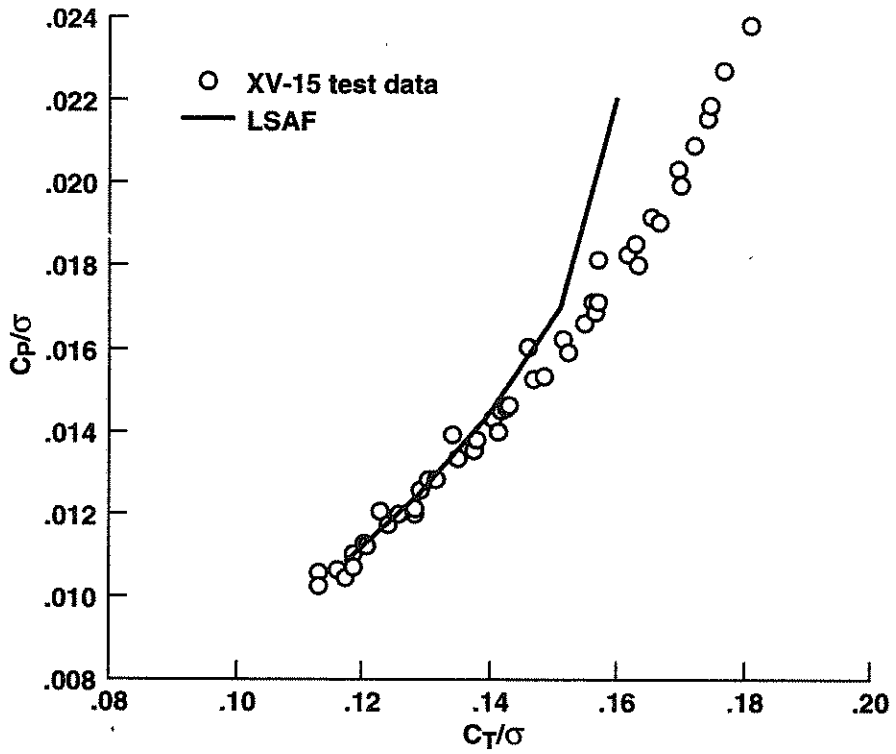

Figure 11(a). Comparison of LSAF hover performance predictions with XV-15 rotor test data.

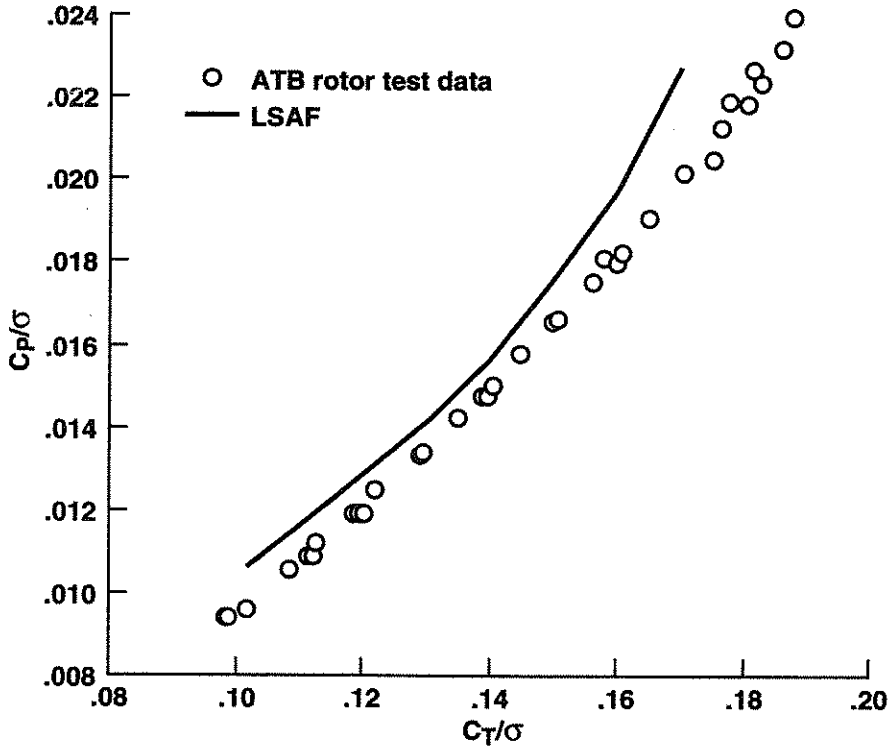

Figure 11(b). Comparison of LSAF hover performance predictions with ATB rotor test data.

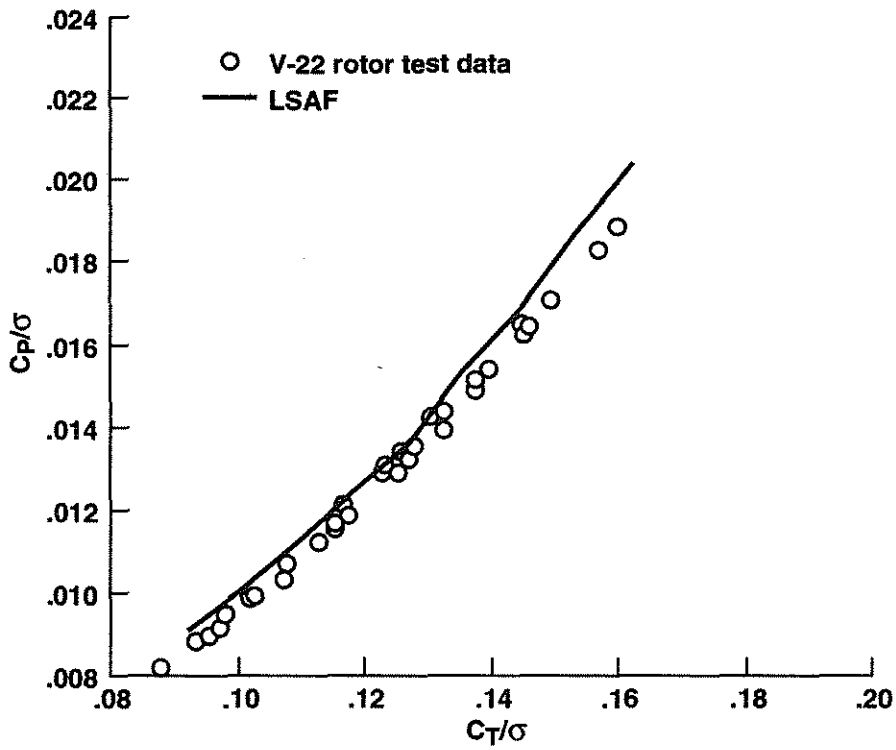

Figure 11(c). Comparison of LSAF hover performance predictions with V-22 rotor test data.

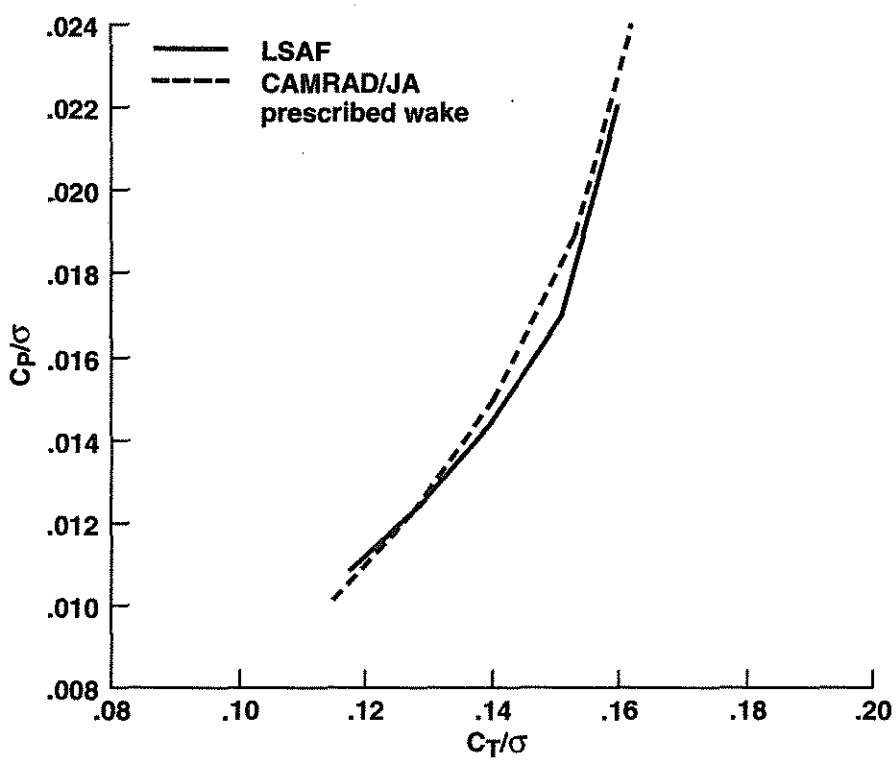

Figure 12(a). Comparison of LSAF and CAMRAD/JA prescribed wake hover performance predictions. XV-15 rotor.

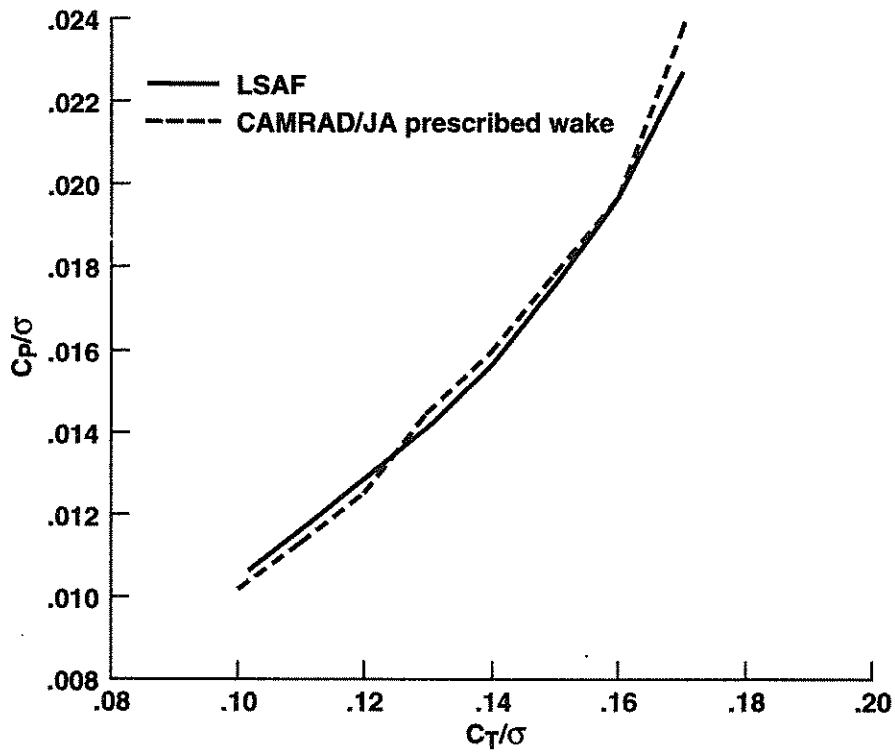

Figure 12(b). Comparison of LSAF and CAMRAD/JA prescribed wake hover performance predictions. ATB rotor.

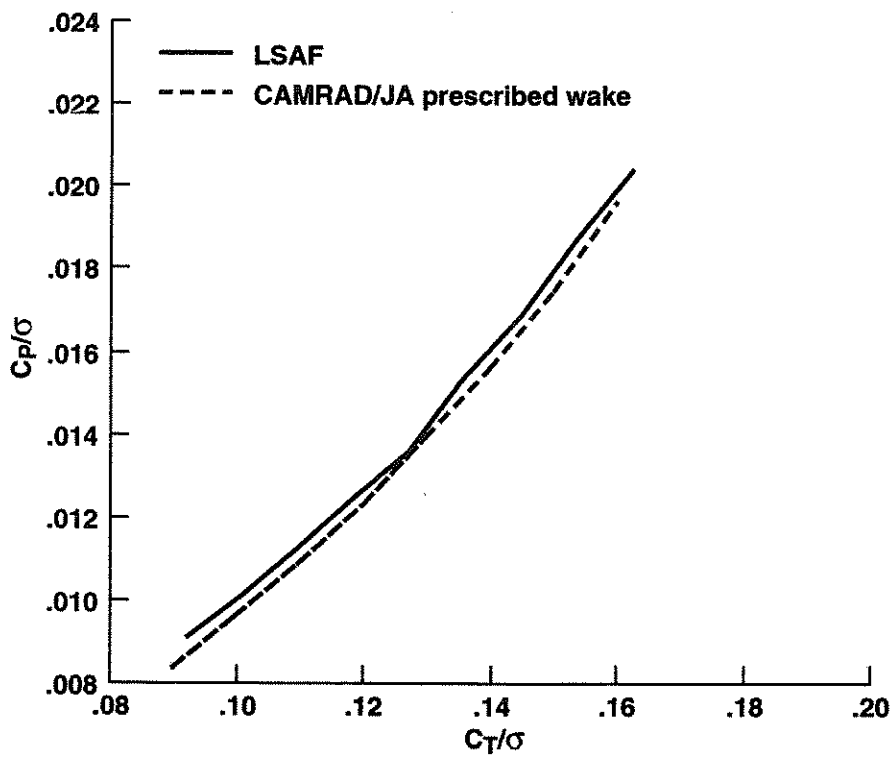

Figure 12(c). Comparison of LSAF and CAMRAD/JA prescribed wake hover performance predictions. V-22 rotor.

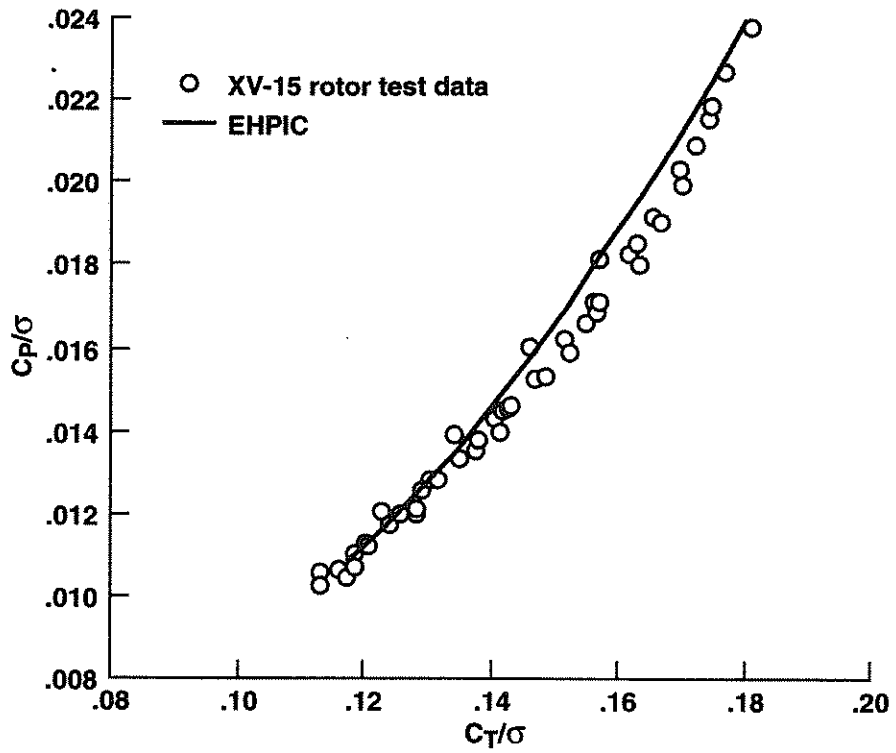

Figure 13(a). Comparison of EHPIC hover performance predictions with XV-15 rotor test data.

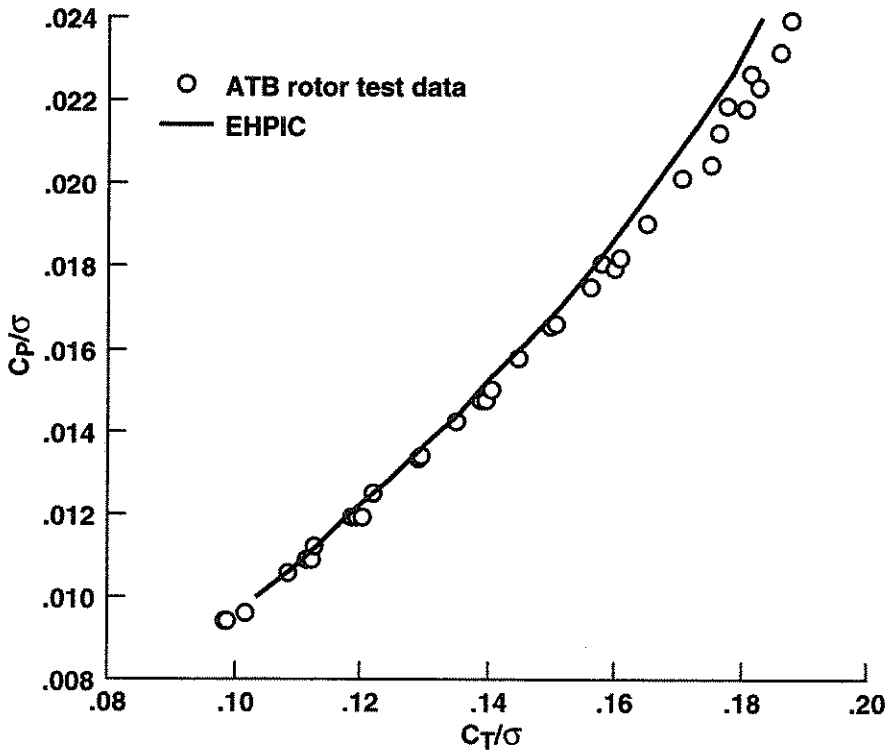

Figure 13(b). Comparison of EHPIC hover performance predictions with ATB rotor test data.

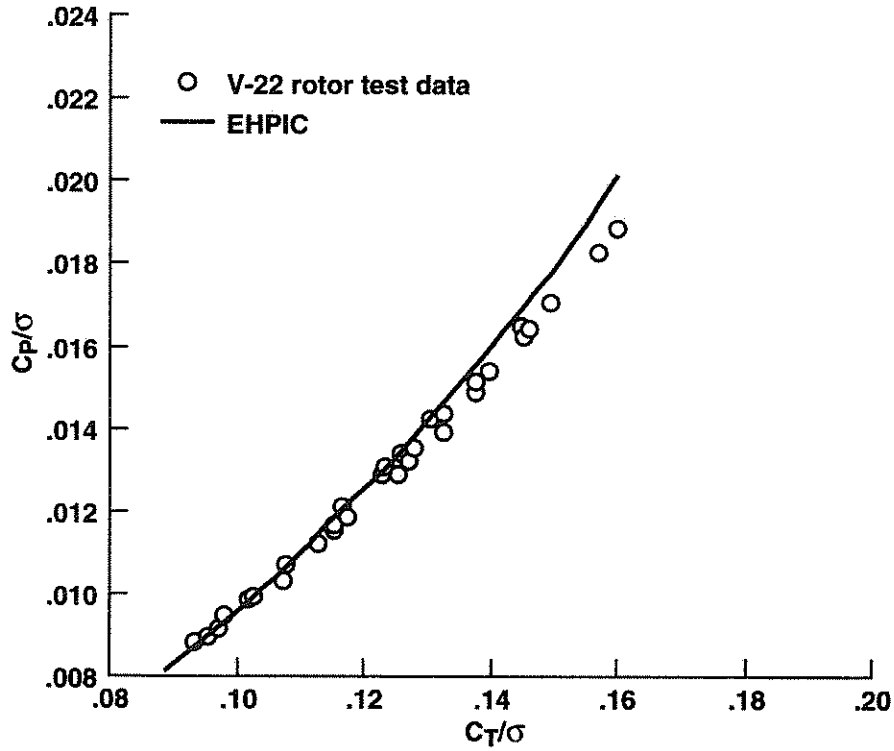

Figure 13(c). Comparison of EHPIC hover performance predictions with V-22 rotor test data.

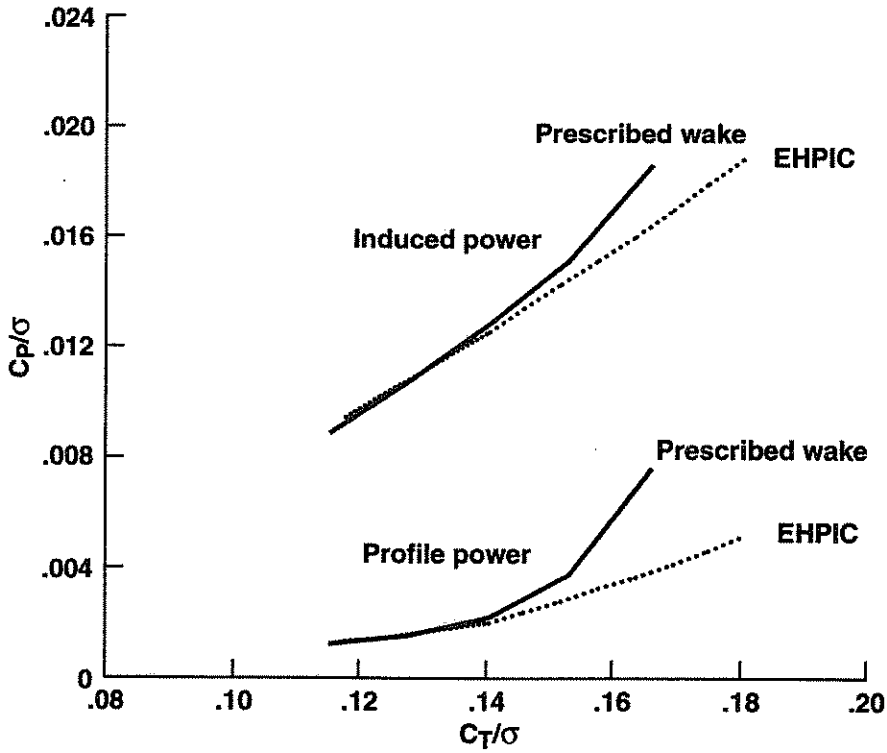

Figure 14. Comparison of induced and profile power predicted using EHPIC and CAMRAD/JA with prescribed wake. XV-15 rotor.

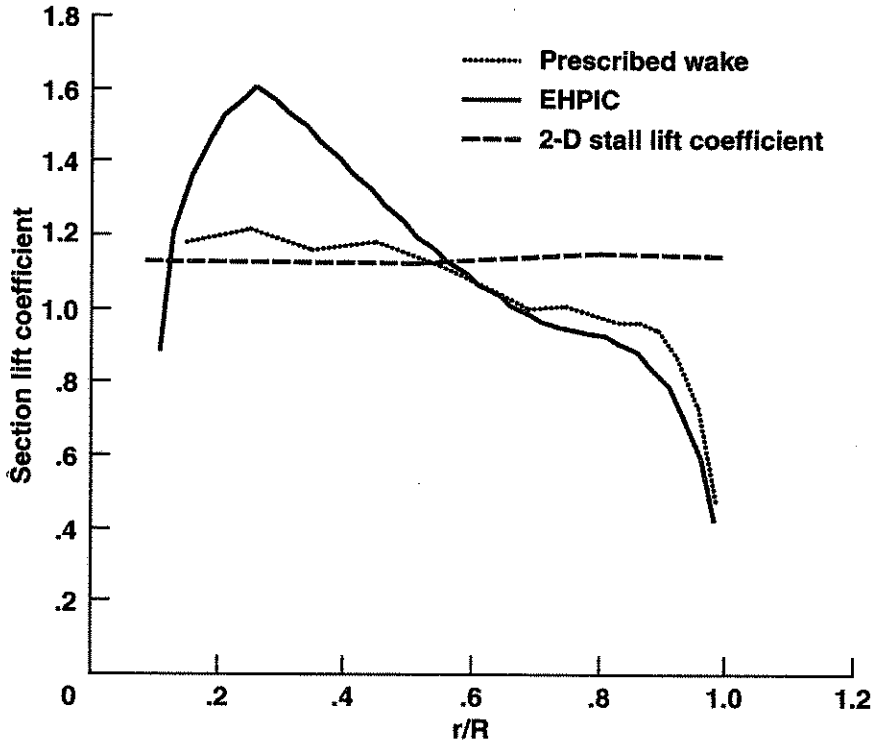

Figure 15. Comparison of sectional lift coefficients predicted by EHPIC and CAMRAD/JA with maximum lift coefficient from 2-D airfoil data. XV-15 rotor, $C_T/\sigma = 0.153$.

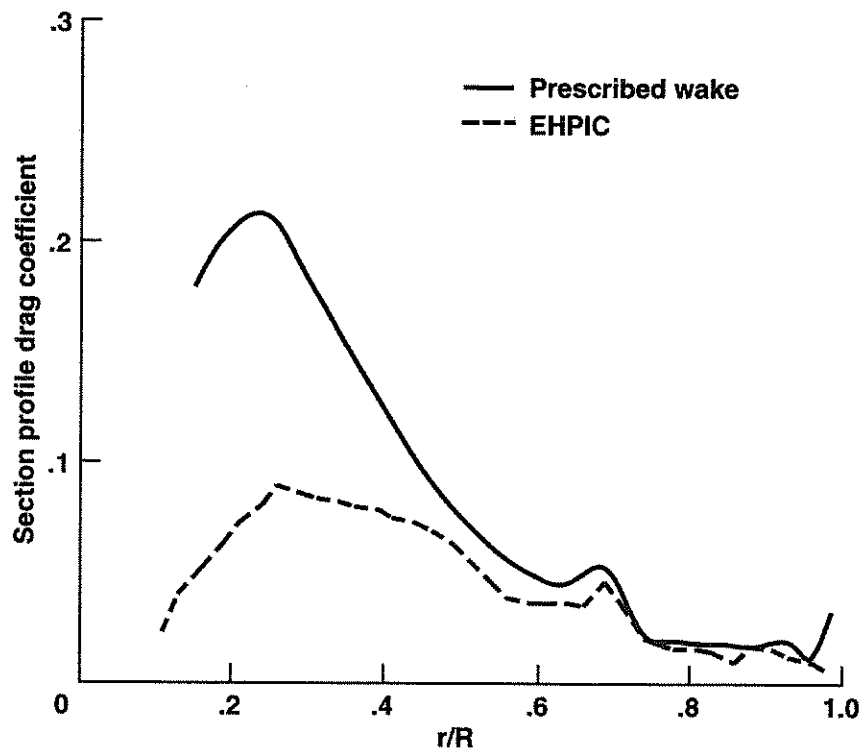

Figure 16. Comparison of sectional drag coefficients predicted by EHPIC and CAMRAD/JA . XV-15 rotor, $C_T/\sigma = 0.153$.

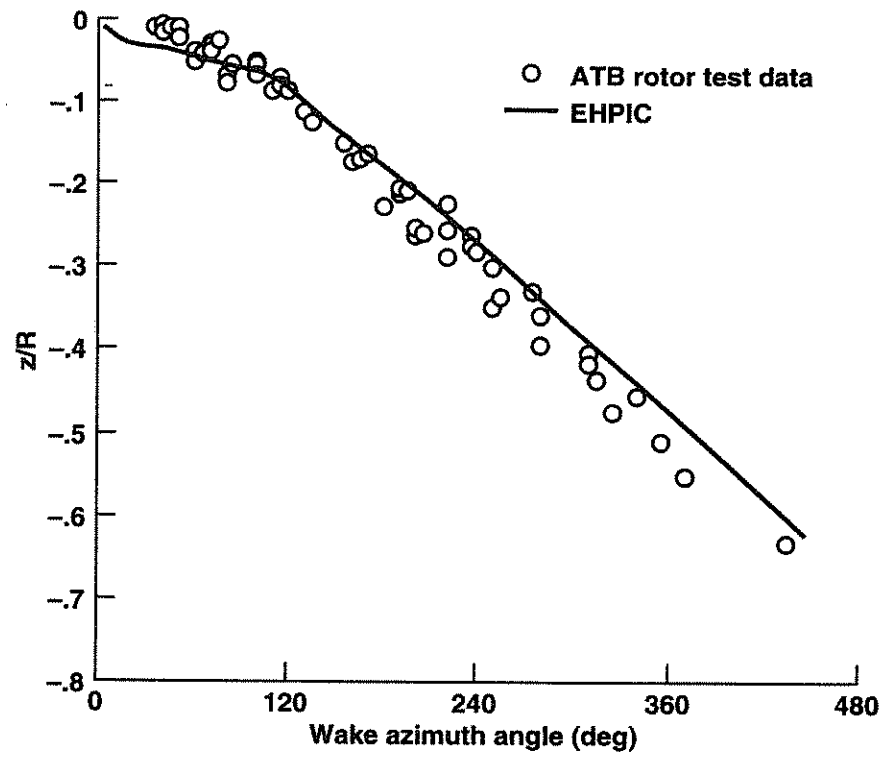

Figure 17(a). Comparison of EHPIC tip vortex axial geometry with test data. ATB rotor, $C_T/\sigma = 0.17$.

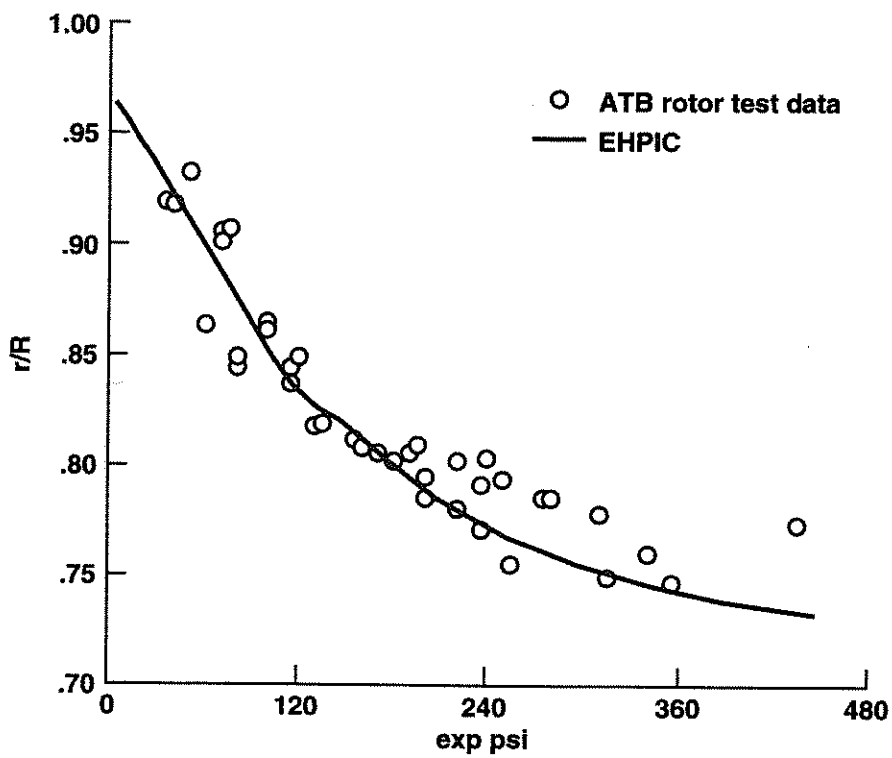

Figure 17(b). Comparison of EHPIC tip vortex radial geometry with test data. ATB rotor, $C_T/\sigma = 0.17$.

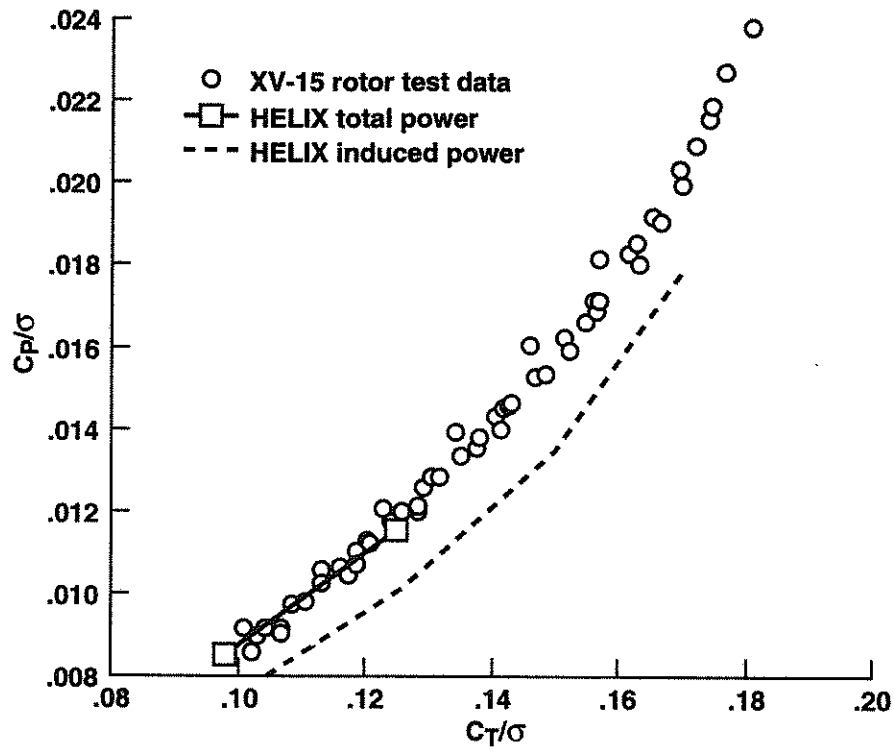

Figure 18(a). Comparison of HELIX hover performance predictions with XV-15 rotor test data.

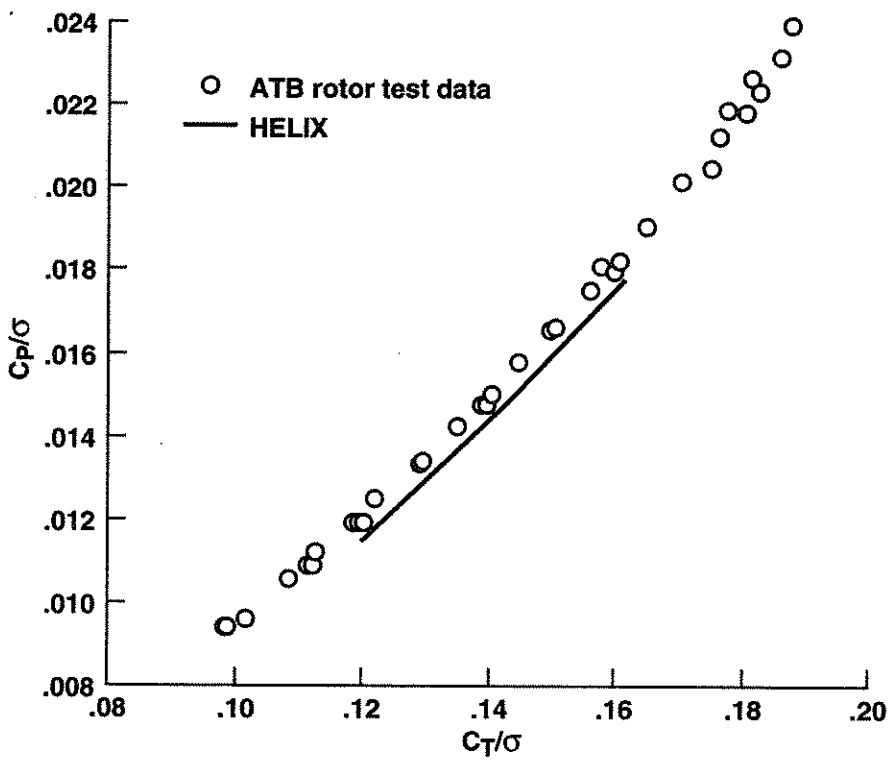

Figure 18(b). Comparison of HELIX hover performance predictions with ATB rotor test data.

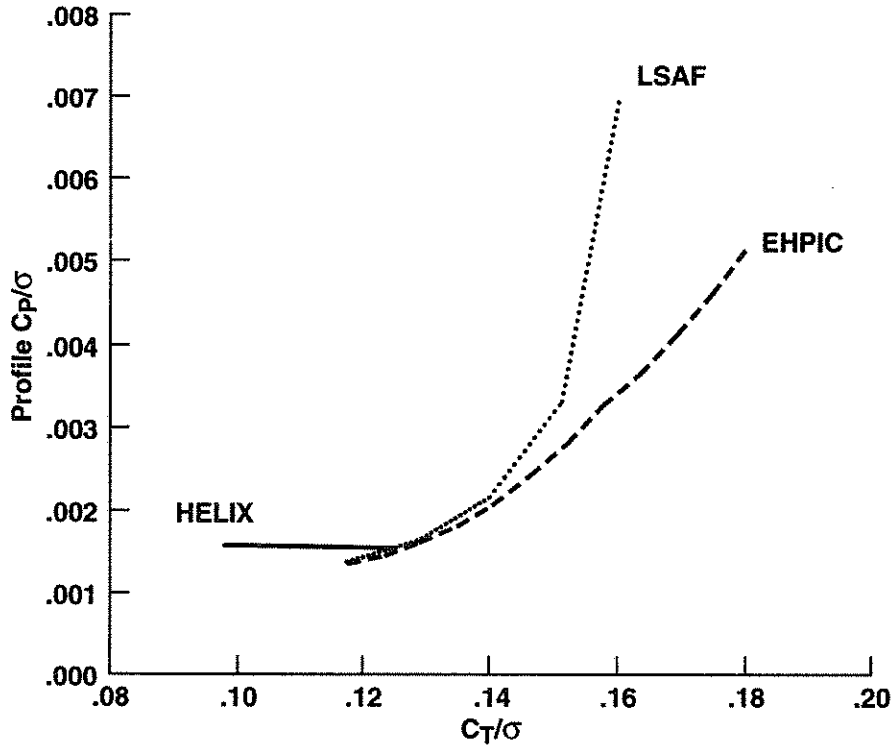

Figure 19(a). Comparison of profile power predicted using various analytical methods. XV-15 rotor.

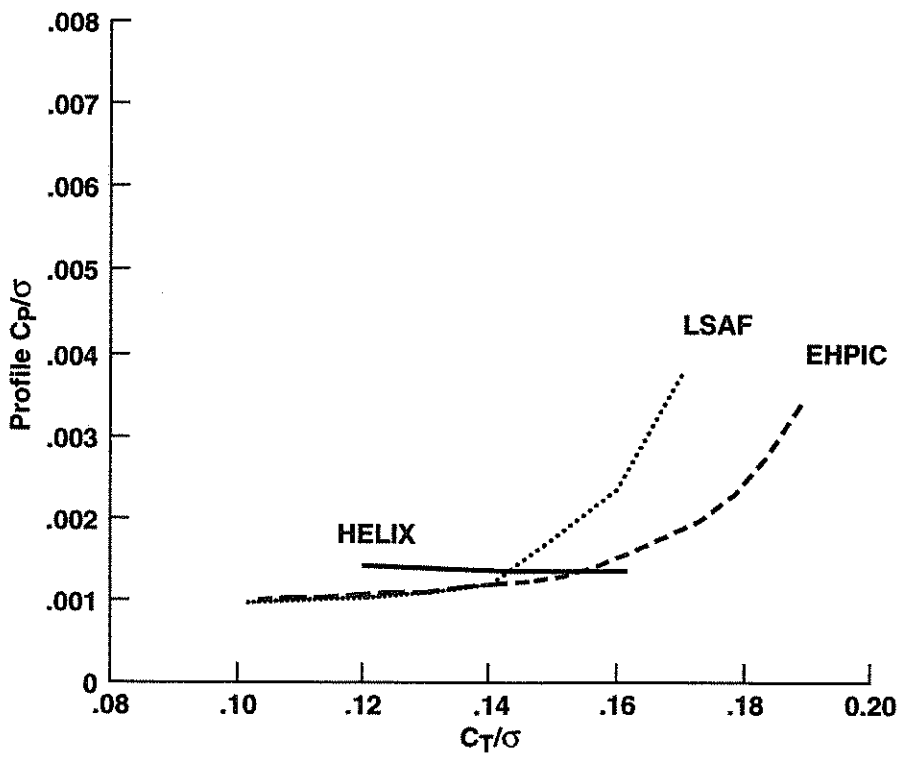

Figure 19(b). Comparison of profile power predicted using various analytical methods. ATB rotor.

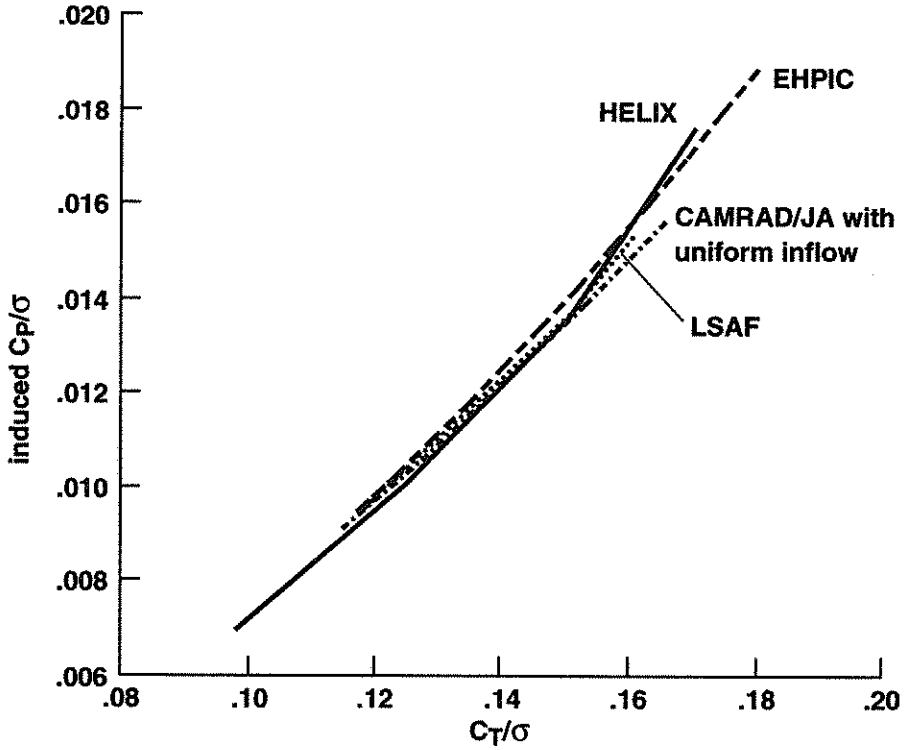

Figure 20. Comparison of induced power predicted using various analytical methods. XV-15 rotor.

REPORT DOCUMENTATION PAGE

Form Approved
OMB No. 0704-0188

Public reporting burden for this collection of information is estimated to average 1 hour per response, including the time for reviewing instructions, searching existing data sources, gathering and maintaining the data needed, and completing and reviewing the collection of information. Send comments regarding this burden estimate or any other aspect of this collection of information, including suggestions for reducing this burden, to Washington Headquarters Services, Directorate for Information Operations and Reports, 1215 Jefferson Davis Highway, Suite 1204, Arlington, VA 22202-4302, and to the Office of Management and Budget, Paperwork Reduction Project (0704-0188), Washington, DC 20503.

1. AGENCY USE ONLY *(Leave blank)*	2. REPORT DATE	3. REPORT TYPE AND DATES COVERED
	June 1993	Technical Memorandum

4. TITLE AND SUBTITLE
Accuracy of Tilt Rotor Hover Performance Predictions

5. FUNDING NUMBERS
532-06-37

6. AUTHOR(S)
Fort F. Felker

7. PERFORMING ORGANIZATION NAME(S) AND ADDRESS(ES)
Ames Research Center
Moffett Field, CA 94035-1000

8. PERFORMING ORGANIZATION REPORT NUMBER
A-93083

9. SPONSORING/MONITORING AGENCY NAME(S) AND ADDRESS(ES)
National Aeronautics and Space Administration
Washington, DC 20546-0001

10. SPONSORING/MONITORING AGENCY REPORT NUMBER
NASA TM-104023

11. SUPPLEMENTARY NOTES
Point of Contact: Fort F. Felker, Ames Research Center, MS T-42, Moffett Field, CA 94035-1000
(415) 604-6096

12a. DISTRIBUTION/AVAILABILITY STATEMENT
Unclassified — Unlimited

12b. DISTRIBUTION CODE

13. ABSTRACT *(Maximum 200 words)*

The accuracy of various methods used to predict tilt rotor hover performance was established by comparing predictions with large-scale experimental data. A wide range of analytical approaches were examined. Blade lift was predicted with a lifting line analysis, two lifting surface analyses, and by a finite-difference solution of the full potential equation. Blade profile drag was predicted with two different types of airfoil tables and an integral boundary layer analysis. The inflow at the rotor was predicted using momentum theory, two types of prescribed wakes, and two free wake analyses. All of the analyses were accurate at moderate thrust coefficients. The accuracy of the analyses at high thrust coefficients was dependent upon their treatment of high sectional angles of attack on the inboard sections of the rotor blade. The analyses which allowed sectional lift coefficients on the inboard stations of the blade to exceed the maximum observed in two-dimensional wind tunnel tests provided better accuracy at high thrust coefficients than those which limited lift to the maximum two-dimensional value. These results provide tilt rotor aircraft designers guidance on which analytical approaches provide the best results, and the level of accuracy which can be expected from the best analyses.

14. SUBJECT TERMS
Tilt rotor, Rotor performance, Aircraft design

15. NUMBER OF PAGES
28

16. PRICE CODE
A03

17. SECURITY CLASSIFICATION OF REPORT	18. SECURITY CLASSIFICATION OF THIS PAGE	19. SECURITY CLASSIFICATION OF ABSTRACT	20. LIMITATION OF ABSTRACT
Unclassified	Unclassified		